Journal of Constructional Steel Research 194 (2022) 107298

Contents lists available at ScienceDirect

Journal of Constructional Steel Research

journal homepage: www.elsevier.com/locate/jcsr

# System reliability-based design of steel-concrete composite frames with CFST columns and composite beams

Hau Tran [a], Huu-Tai Thai [a,*], Brian Uy [b], Stephen J. Hicks [c], Won-Hee Kang [d]

[a] Department of Infrastructure Engineering, The University of Melbourne, Parkville, VIC 3010, Australia
[b] School of Civil Engineering, The University of Sydney, Sydney, NSW 2006, Australia
[c] School of Engineering, The University of Warwick, Coventry CV4 7AL, UK
[d] School of Engineering, Design and Built Environment, Western Sydney University, Penrith, NSW 2751, Australia

ARTICLE INFO

*Keywords:*
CFST column
Monte Carlo method
Steel-concrete composite frame
Subset simulation
System resistance factor
Reliability analysis

ABSTRACT

This paper presents an effective reliability analysis procedure and proposes the system resistance factors for the system design of steel-concrete composite frames that comprise of concrete-filled steel tubular (CFST) columns and composite beams. Advanced analysis is employed to predict the ultimate resistance of frames using fibre beam-column elements in OpenSees. The obtained predictions of the load-carrying capacity of frames compare well with experimental results with the mean value of the test-to-prediction ratio around 1.027 and the coefficient of variation (*CoV*) of 8.4%. Both Monte Carlo (MC) and subset simulations are used in the reliability analysis. The uncertainties of model error, geometric and material properties, and external loads are included to predict the system reliability index. Five different frame configurations are considered. The results of the reliability analysis show that the system resistance factors for both US and AS codes are quite similar. In the case of gravity load, the system resistance factor is from 0.78 to 0.90, whilst this value for the case of combined wind and gravity load is from 0.8 to 0.95. The resistance factors suggested herein become valuable reference information for the system design of composite frames.

## 1. Introduction

In recent years, steel-concrete composite structures that comprise of concrete filled steel tubes/plates and steel-concrete composite beams have drawn great attention from researchers [1–10]. In comparison to reinforced concrete (RC) structures, steel frames/buildings or other composite systems, concrete filled steel tubes/plates structures have demonstrated superior advantages such as faster construction speed, better ductility and higher load-carrying capacity, which leads to their popularity in practice [11–13]. Conventionally, these structures are designed by the load resistance factor design (LRFD) given in the design provisions of some codes such as AISC 360–16 [14] and AS/NZS 2327 [15]. In this approach, the internal forces for the design are normally extracted from the elastic analysis and implemented into the design equations in which material capacity factors are considered to predict the load-carrying capacity of each member.

Although the concept of LRFD is acceptable, it still has some disadvantages such as: (1) each element is considered as an isolated member since it works as a part of the whole system in practice, therefore, the initiation and the distribution of plasticity in the system are not captured; and (2) the structure is considered to fail if one element fails leading to a conservative design. In contrast, the system design is based on nonlinear inelastic analysis that considers both the material and the geometric nonlinearities. Therefore, it can overcome the limitations mentioned above [16] and can accurately reflect the practical behaviour of the designed structures.

By applying this method, the designed resistance of the composite frame can be simply determined by multiplying the system resistance factor found from system reliability analysis with the ultimate load-carrying capacity obtained directly from nonlinear inelastic simulations. As a result, the requirement to check the capacity of each isolated member of the structure is no longer necessary in the system-based design approach. In addition, the system-based design also makes the structures lighter leading to a more economical design. For example, as mentioned in the study by Ziemian et al. [17], the design by advanced analysis can save around 12% of steel weight in comparison to traditional LRFD design. Due to those advantages, a variety of studies have focused on the nonlinear analysis for the system design and system

* Corresponding author.
*E-mail address:* tai.thai@unimelb.edu.au (H.-T. Thai).

https://doi.org/10.1016/j.jcsr.2022.107298
Received 4 November 2021; Received in revised form 17 April 2022; Accepted 20 April 2022

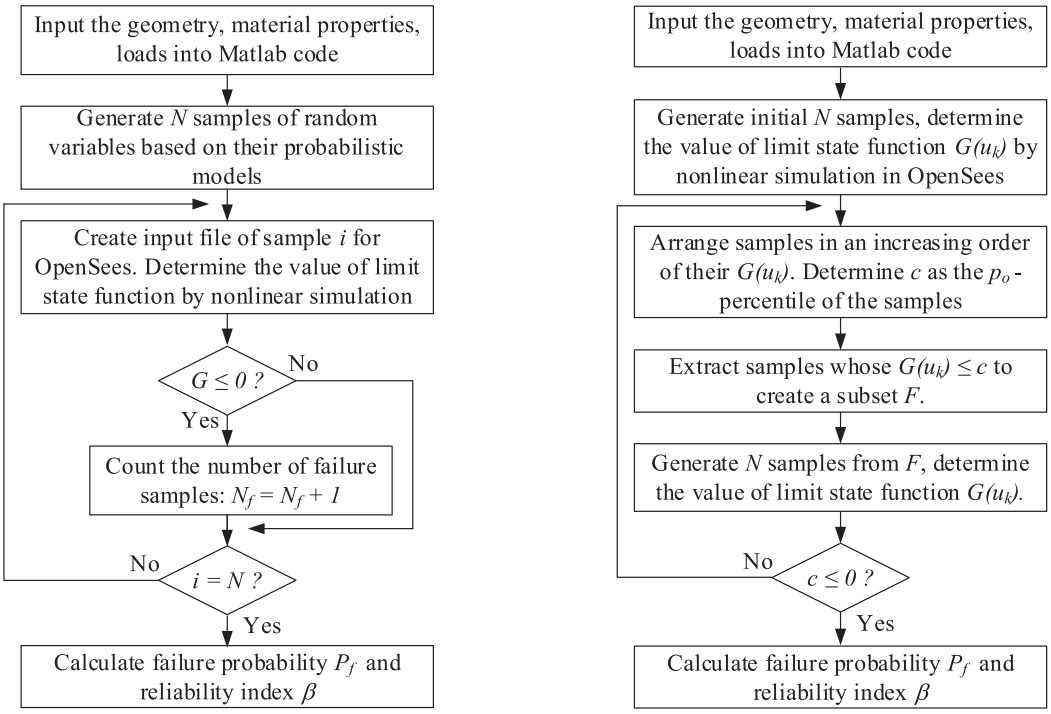


**Fig. 1.** Reliability analysis based on MC method and subset simulation.

reliability of structures [16,18–22] in which significant efforts have been made to develop the nonlinear inelastic simulation for the whole system such as composite buildings with CFST columns and innovative coupling composite shear walls [7]. However, the system resistance factor, especially the one for steel-concrete composite structures, is still lacking information.

Regarding the system reliability, great attention from researchers has been drawn since it was found that the properties of materials, section dimensions and external loads in a structure and the accuracy of the numerical models are uncertain. Considering these uncertainties, the likelihood of the failure and the safe states of a structure need to be represented by probabilistic measures such as a failure probability and a reliability index. There are plenty of approaches that have been applied to conduct reliability analysis such as first-order reliability method (FORM) [16,23], MC method [22,24], subset simulation [25,26], line-sampling-method-based slime mold algorithm (LS-SMA) [27], and Latinised partially stratified sampling and efficient importance sampling (LPSS-EIS) [20]. Thai et al. [22] employed the MC method to investigate the reliability of planar frames. Although their study provided comprehensive results on the behaviour and reliability of frames with semi-rigid connections, it only focused on steel frames. In the study by Zhang et al. [16], the procedure for the assessment of system reliability indices and system resistance factors was proposed by utilizing the FORM method. However, their study was also limited to steel structures and the results based on FORM were not accurate enough, especially for highly nonlinear structures like steel and composite frames. Keshtegar et al. [28] used artificial intelligence to enhance the computational efficiency of FORM, but the application of this approach to complex and highly nonlinear composite structures was not performed in their study.

Notwithstanding this, some studies about the reliability of composite structures can be found in the literature [26,29–31]. Chen et al. [30] proposed the system resistance factors for the CFST truss structures that are applicable to the design of bridges rather than frames and buildings. Whilst Thai et al. [26] and Beck et al. [29] only assessed the reliability of CFST columns designed by provisions from various standards. Hence, a comprehensive study on the system reliability of the steel-concrete composite frames with CFST columns has not been available yet.

The present study aims to fill such gaps by developing a highly effective analysis procedure with less computational cost to evaluate the system reliability and propose the system resistance factors of 2D steel-concrete composite frames with CFST columns and composite beams. All uncertainties in model error, loading and material and geometric properties are considered in the proposed procedure using both MC and subset simulations. MATLAB codes are developed to automatically generate input files of composite frames with random properties used for the advanced analysis in the OpenSees software. After that, five different frame configurations with compact and non-compact sections are investigated. These frames are subjected to two loading scenarios which are only gravity load or combined wind and gravity loads with the column strength-to-beam strength ratio fluctuating in the range from 0.8 to 1.7 or 0.5 to 1.2, respectively. Finally, an extensive parametric study is conducted to determine the system resistance factors for the system-based design of composite frames.

## 2. System reliability analysis

The structural design is to assure that the load-carrying capacity of the designed structures is not lower than the total applied loads to make these structures safe and functionally operational. In the design phase, the nominal characteristics of materials, loads and dimensions are employed. However, these values are not constant due to the existence of uncertainties, which are represented as random variables. The probability of failure of a structure is related to its reliability index by the following equation:

$$\beta = -\Phi^{-1}(P_f) \tag{1}$$

where $\Phi$ is the standard normal cumulative distribution function, and $P_f$ is the probability of failure that can be calculated by the methods mentioned below.

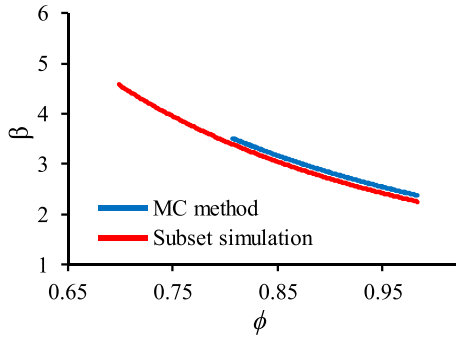


**Fig. 2.** Comparison between subset simulation and MC method.

**Table 1**
Comparison between subset and MC method for frame 1.

| $\phi$ | $\beta$ | | Error (%) | Computing time (hour) | |
|---|---|---|---|---|---|
| | Subset simulation | MC simulation | | Subset simulation | MC simulation |
| 0.983 | 2.280 | 2.390 | 4.60 | 1.12 | 3.95 |
| 0.944 | 2.480 | 2.640 | 6.06 | 3.14 | 7.12 |
| 0.890 | 2.910 | 3.030 | 3.96 | 1.18 | 49.53 |
| 0.847 | 3.150 | 3.230 | 2.48 | 2.23 | 65.91 |
| 0.807 | 3.420 | 3.460 | 1.16 | 0.87 | 110.63 |

The simplest method to calculate the failure probability is the FORM method, but it is not accurate when applied in complex structures with high nonlinearity or multiple limit states [20]. Therefore, this study uses simulation-based methods including MC method and subset simulation to conduct reliability analysis of steel-concrete composite structures. These two approaches are applied in the study because MC simulation is the most reliable and widely accepted method among those used for the reliability analysis of highly nonlinear structures whose the limit state function cannot be explicitly defined [32], whilst subset simulation is a simple and efficient approach [25]. In the MC method, the random variables are generated based on their statistical distributions. For each simulation, the advanced analysis is conducted to determine the load-carrying capacity of each structure (see Fig. 1a). The failure probability of the structure is then calculated by the following equation:

$$P_f = \frac{N_f}{N} \tag{2}$$

where $N_f$ is the number of failure samples, and $N$ is the total number of the generated samples. To evaluate whether a sample fails, the following limit state function is used:

$$G(X_i, Y_i) = ME \times R(X_i, Y_i)/Q(Y_i) - 1 \tag{3}$$

in which $ME$ is the model error obtained from Section 4.1, $R$ is the load-carrying capacity of the current sample which is dependent on random variables $X_i$ and $Y_i$ presented in Table 3, $X_i$ are random variables for material and geometrical properties, $Y_i$ are random variables for nominal applied loads, and $Q$ is the total nominal applied loads. In the case of gravity load, $R$ is the gravity resistance of the generated sample, and $Q = D_n + L_n$ (i.e., a total of dead load $D_n$ and live load $L_n$). When the structure is subjected to combined wind and gravity loads, $R$ is the lateral load-carrying capacity of the sample, and $Q$ is taken as the total applied wind load ($W_n$).

The concept of the MC method is relatively straightforward and feasible to apply in any practical structures. However, when the failure probability is small, a large number of samples are required to achieve reliable results, which leads to highly computational cost. The convergence of the failure probability obtained from the MC method is represented by the $CoV$ as shown in the following equation [33]:

$$CoV = \sqrt{\frac{1 - P_f}{NP_f}} \tag{4}$$

Due to this disadvantage, subset simulation proposed by Au and Beck [34] is adopted when the reliability index is larger than 3.5 to save computational time. In this approach, a subset from the initial samples is extracted. The values of the limit state functions of all samples in the subset are smaller than the $p_o$-percentile of the initial samples, where $p_o$ is the probability of intermediate subsets that can be taken as 0.1 [34]. The extracted subset is then used to generate new samples by employing the adaptive conditional sampling technique (see Fig. 1b) proposed by Papaioannou et al. [25]. The details of the subset simulation procedure applied in the reliability analysis of CFST frames in this paper are presented as follows:

(a) Generate the $N$ initial samples $\{u_k: k = 1, \ldots, N\}$ based on the probabilistic models. Each sample consists of random values of variables such as model error, applied load, etc. The value of the limit state function corresponding to each sample is then determined by a nonlinear analysis $\{G(u_k): k = 1, \ldots, N\}$.
(b) Arrange the samples $\{u_k: k = 1, \ldots, N\}$ in an increasing order of the values of limit state functions. Find $c_j$ as the $p_o$ – percentile of the samples $\{G(u_k): k = 1, \ldots, N\}$. Extract samples whose values of limit state functions are not larger than $c$ ($G(u_k) \le c$) to create a subset $F = \{u_k: k = 1, \ldots, N_S\}$.
(c) Utilize adaptive conditional sampling technique to generate $N$ samples $\{u_k: k = 1, \ldots, N\}$ from the subset $F$ extracted in the previous step. Conduct nonlinear analysis to find the value of limit state function of each sample $\{G(u_k): k = 1, \ldots, N\}$.
(d) Steps (b) and (c) are iterated until $c < 0$. Then identify $N_f$ of the samples $\{u_k: k = 1, \ldots, N\}$ in the last iteration, and calculate the failure probability by the following equation:

$$P_f = p_0^j \frac{N_f}{N} \tag{5}$$

where $N_f$ is the number of failure samples, and $j$ is the number of loops.

It can be seen from Fig. 2 that the relationship between $\beta$ and $\phi$ of frame 1, which is a 3-story 1-bay steel-concrete composite frame subjected to combined wind and gravity loads (more information of this frame can be found Section 5), obtained from subset simulation is close to the curve obtained from the MC method. It should be noted that the $\beta - \phi$ curve in the case of MC method is shorter because when the reliability index is higher than 3.5, the number of samples required to yield good results is substantially large leading to extremely long calculation time (see Table 1). Therefore, those cases are neglected. In Table 1, the comparison between MC method and subset simulation on the reliability indices and their calculation time is illustrated. It is obvious that the reliability indices calculated from two methods agree well with each other while the discrepancy is less than 6%, which demonstrates that the developed MATLAB codes are reliable. Table 1 also shows the efficiency of subset simulation since it can significantly reduce the calculation time of the reliability analysis in comparison to that of the MC method.

## 3. System resistance factors

In the system-based design approach, the designed load-carrying capacity of the structure should not be smaller than the total applied loads as follows:

$$\phi R \ge \sum \gamma_i Q_i \tag{6}$$

where $\phi$ is the system resistance factor or the system capacity factor that needs to be determined; $R$ is the system load-carrying capacity obtained from nonlinear simulation; $Q_i$ are the applied loads and $\gamma_i$ are the load factors given in design codes. Equating the left side of Eq. (6) to the right

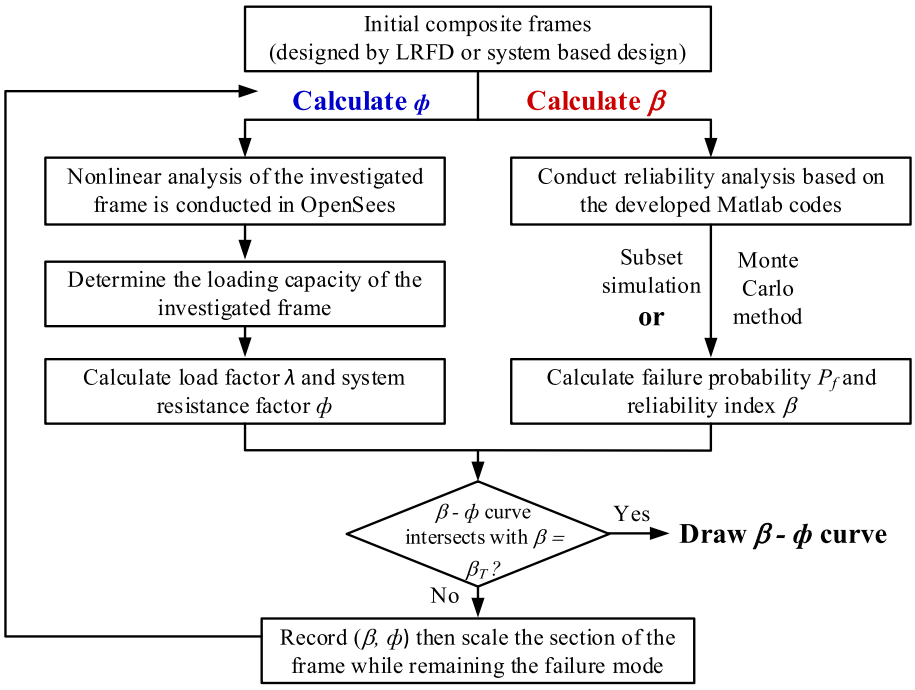


**Fig. 3.** Procedure to determine system resistance factor.

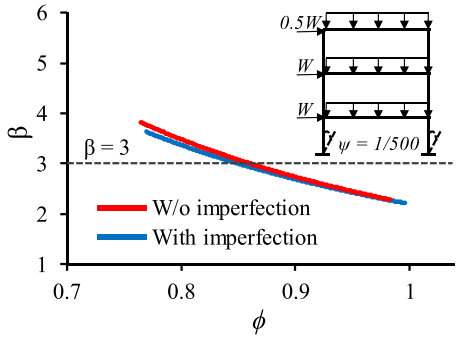


**Fig. 4.** The effect of sway imperfection on the reliability index of frame 1.

side, we have:

$$\frac{1}{\phi} = \frac{R}{\sum \gamma_i Q_i} = \lambda_L \tag{7}$$

where $\lambda_L$ is the load factor. In conventional LRFD approach, the capacity factors for the design of each structural element are provided clearly in national codes (i.e., AS/NZS 2327 [15]), but the provisions for the system resistance factors are still inadequate. In this study, the system resistance factors for composite structures are calculated by conducting the reliability analysis based on the following procedure (see Fig. 3, Tables 6 and 8 for more information):

(i) The composite structures are designed by LRFD or system-based design approach to obtain the reference section dimensions.
(ii) Nonlinear simulation is conducted to determine the load factor $\lambda_L$ and the corresponding system resistance factor $\phi$.
(iii) Reliability analysis is carried out to find the reliability index $\beta$ corresponding to the calculated system resistance factor $\phi$ obtained in step (ii).
(iv) Section dimensions are scaled down if the reliability index $\beta$ of the initial frame is larger than the target reliability index $\beta_T$, and scaled up if $\beta$ is smaller than $\beta_T$. Steps (ii) to (iv) are repeated until the $\beta - \phi$ curve intersects with the horizontal line $\beta = \beta_T$ (see Figs. 13 and 14).
(v) Determine the system resistance factor $\phi$ for the design based on the $\beta - \phi$ relationship and the target reliability index $\beta_T$.

## 4. Probabilistic model for variables

To capture the failure probability of the structure precisely, the uncertainties in model error, section dimensions, material properties and applied loads will be taken into consideration. In typical building structures, the influence of out-of-straightness imperfection is small and the important imperfection is out-of-plumbness (sway imperfection) [6,14]. However, this kind of imperfection also shows negligible effects on the reliability of steel-concrete composite frames investigated in this study (see Fig. 4). Therefore, geometric imperfections are not considered in this paper.

### 4.1. Model error

In this study, the nonlinear analysis of composite frames is conducted using *forceBeamColumn* element in OpenSees with just one element for each structural component. The steel is considered as elastic-perfectly-plastic. The stress-strain relationship of concrete in tension is bilinear, the models of confined and unconfined concrete in compression are also considered rigorously in the study. More details of the simulation procedure of steel-concrete composite structures with CFST columns and composite beams can be found in Tran et al. [7]. In order to capture the reliability of practical structures, the numerical simulation is utilized to model both 2D and 3D frames from numerous studies (Table 2), which includes 37 pairs of $P_{test}/P_{cal}$ to find the model error, where $P_{cal}$ is the predicted resistance using fibre-beam elements (see Fig. 5). These frames are assembled from steel-concrete composite beams and steel columns/CFST columns, steel beams and CFST columns or steel-concrete composite beams and composite shear walls. In addition, these frames are also subjected to various loading conditions including gravity load or combined gravity and static/cyclic lateral loads. The results obtained from the simulations are then compared with those from experiments to determine the statistical distribution of the model error.

**Table 2**
Model error.

| No. | Specimen | Loading phase | $P_{test}$ (kN) | $P_{cal}$ (kN) | Test/Cal. | Reference |
|---|---|---|---|---|---|---|
| 1 | 3D composite frame | Push | 1160.00 | 1184.00 | 0.980 | [37] |
| 2 | 3D composite frame | Pull | −1174.00 | −1158.00 | 1.014 | |
| 3 | Specimen CCE5 | Push | 173.16 | 164.97 | 1.050 | [53] |
| 4 | Specimen CCE5 | Pull | −187.20 | −176.67 | 1.060 | |
| 5 | Specimen CCEW6 | Push | 176.80 | 164.42 | 1.075 | |
| 6 | Specimen CCEW6 | Pull | −159.12 | −141.44 | 1.125 | |
| 7 | Specimen F·C | Push | −276.40 | −266.42 | 1.037 | [36] |
| 8 | Specimen F·C | Pull | 358.70 | 367.65 | 0.976 | |
| 9 | Specimen L.P·C | Push | 336.70 | 278.75 | 1.208 | |
| 10 | Specimen L.P·C | Pull | −389.20 | −373.16 | 1.043 | |
| 11 | Specimen I.P·C | Push | 271.30 | 266.45 | 1.018 | |
| 12 | Specimen I.P·C | Pull | −347.30 | −356.73 | 0.974 | |
| 13 | Specimen FP | Push | 132.00 | 137.30 | 0.961 | [54] |
| 14 | Specimen FP | Pull | −149.00 | −129.12 | 1.154 | |
| 15 | 2-Story 2-bay composite frame | – | 195.00 | 203.95 | 0.956 | [55] |
| 16 | Composite planar frame | – | 145.00 | 143.38 | 1.011 | [56] |
| 17 | Specimen DSCW4 | Push | 880.00 | 784.60 | 1.122 | [57] |
| 18 | Specimen DSCW4 | Pull | −750.00 | −770.30 | 0.974 | |
| 19 | Specimen DSCW5 | Push | 1370.00 | 1245.62 | 1.100 | |
| 20 | Specimen DSCW5 | Pull | −1325.00 | −1239.20 | 1.069 | |
| 21 | Composite space frame-beam 1 | Beam 1 | 578.50 | 619.90 | 0.933 | [58] |
| 22 | Composite space frame-beam 2 | Beam 2 | 528.60 | 570.30 | 0.927 | |
| 23 | Composite space frame-beam 3 | Beam 3 | 549.60 | 585.50 | 0.939 | |
| 24 | Specimen CF1 | Push | 515.00 | 530.22 | 0.971 | [35] |
| 25 | Specimen CF1 | Pull | −575.00 | −632.40 | 0.909 | |
| 26 | Specimen CF2 | Push | 441.00 | 434.58 | 1.015 | |
| 27 | Specimen CF2 | Pull | −462.00 | −424.93 | 1.087 | |
| 28 | Specimen SFH2 | Push | 301.00 | 295.90 | 1.017 | [59] |
| 29 | Specimen SFH2 | Pull | −321.00 | −283.50 | 1.132 | |
| 30 | Composite frame | Push | 450.00 | 472.71 | 0.952 | [60] |
| 31 | Composite frame | Pull | −420.00 | −460.47 | 0.912 | |
| 32 | Specimen NR3 | – | 254.00 | 292.25 | 0.869 | [61] |
| 33 | Specimen SF21 | – | 162.00 | 140.00 | 1.157 | [62] |
| 34 | Composite frame 1 | Push | 142.00 | 153.04 | 0.928 | [63] |
| 35 | Composite frame 1 | Pull | −155.00 | −142.94 | 1.084 | |
| 36 | Composite frame 3 | Push | 590.00 | 571.02 | 1.033 | [63] |
| 37 | Composite frame 3 | Pull | −690.00 | −567.24 | 1.216 | |
| Mean | | | | | 1.027 | |
| *CoV* | | | | | 0.084 | |

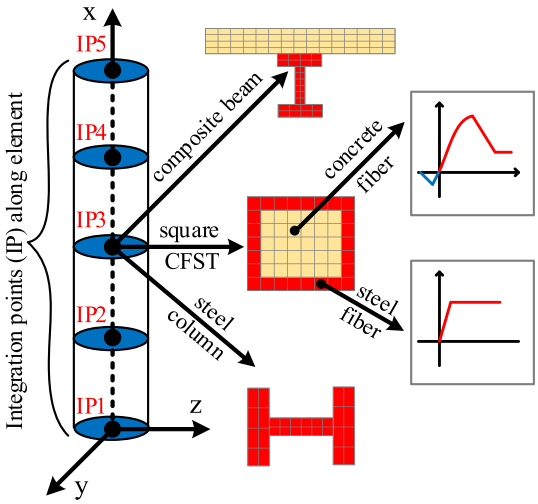


**Fig. 5.** Beam-column element with fibre section.

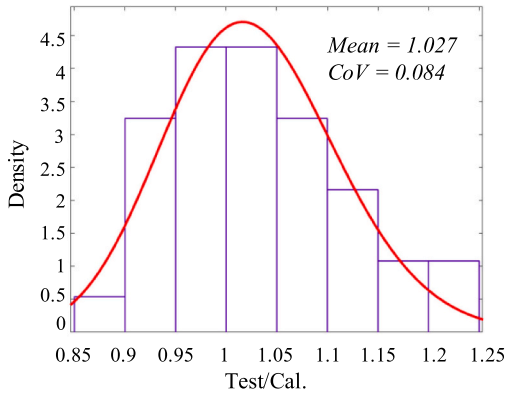


**Fig. 6.** Statistical properties of model error.

In Table 2, the values of load-carrying capacity obtained from test ($P_{test}$) and simulation ($P_{cal}$) of the investigated frames are illustrated. It can be seen that the test-to-prediction ratios ($P_{test}/P_{cal}$) are in the range from 0.85 to 1.2, which is acceptable since this study only employs fibre-beam elements. After the fitting procedure using MATLAB, it has been found that lognormal distribution is the best fit to the obtained test-to-prediction ratios (see Fig. 6) with the mean and *CoV* around 1.027 and 0.084, respectively. The results of some typical composite frames are demonstrated below.

#### *4.1.1. Steel-concrete composite frame with CFST columns and composite beams/steel beams*

Nie et al. [35] tested full-scale CFST frames, namely CF-1 and CF-2 (Figs. 7a and 8a), to investigate the effect of the concrete slab on the seismic behaviour of these frames. The CFST columns of the frames have the section dimensions of 350 × 330 × 10 mm, fabricated from steel with a yield strength of 337 MPa. The 120-mm-thick composite slab is placed on the top of steel beams of frame CF-1 and connected to these

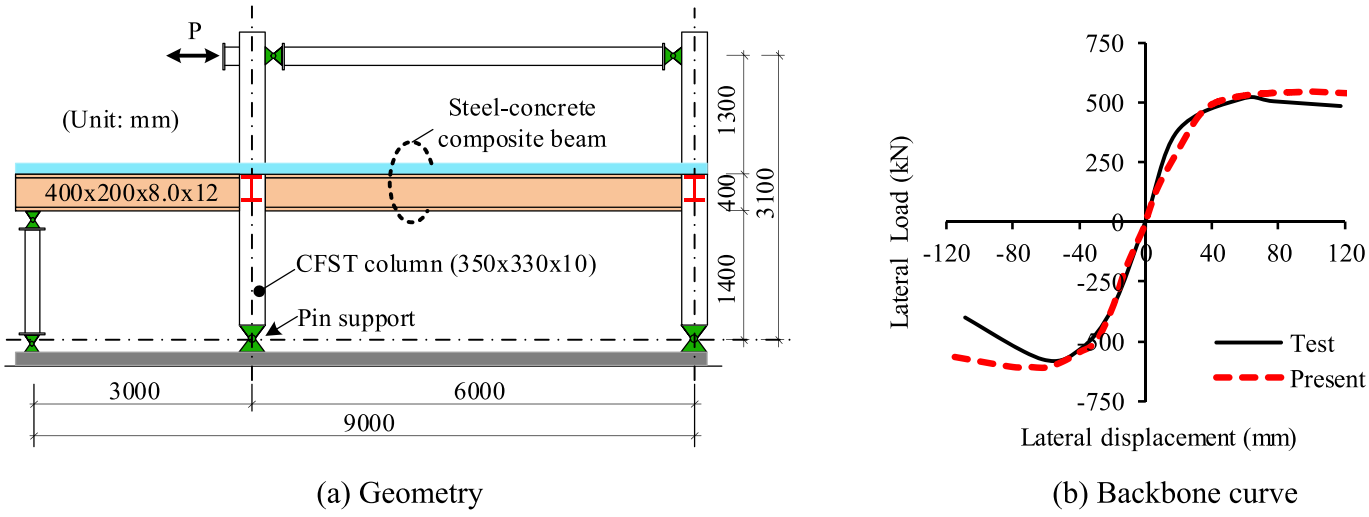


**Fig. 7.** Frame with CFST columns and steel-concrete composite beams [35].

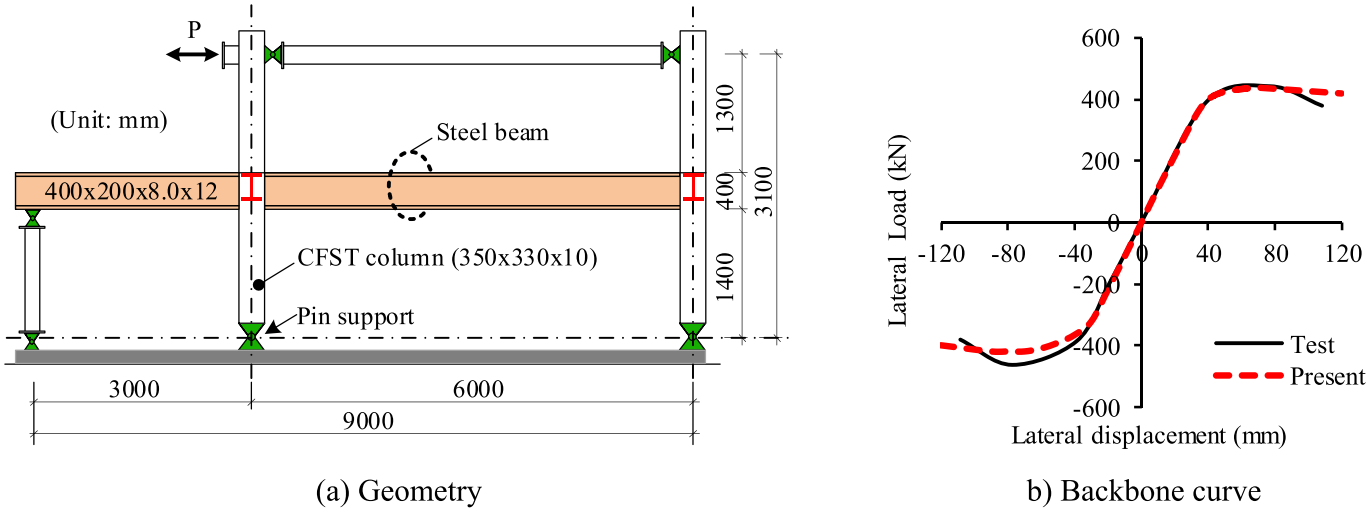


**Fig. 8.** Frame with CFST columns and steel beams [35].

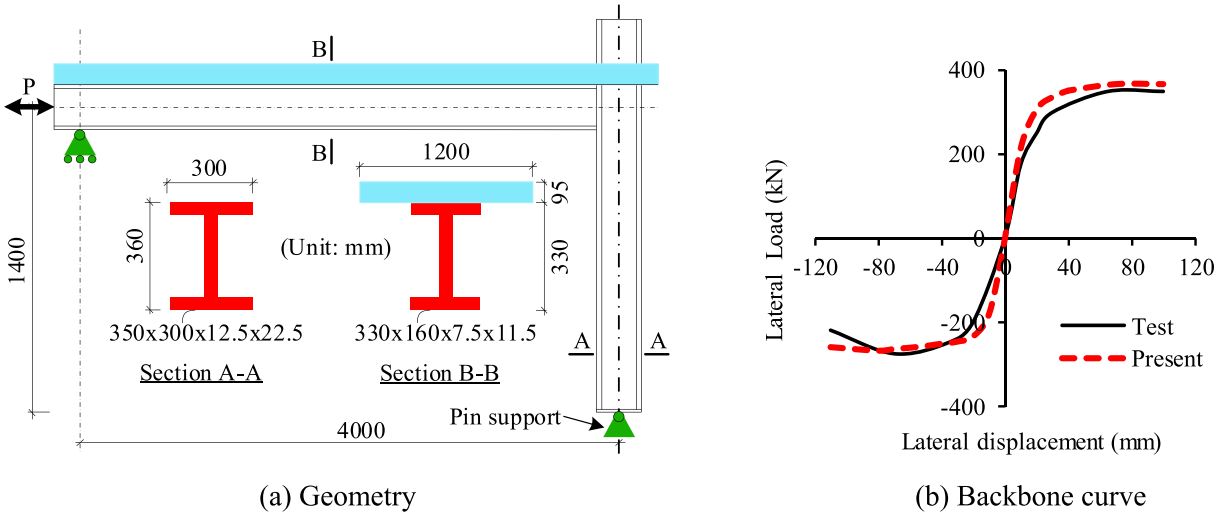


**Fig. 9.** Frame with steel column and steel-concrete composite beams [36].

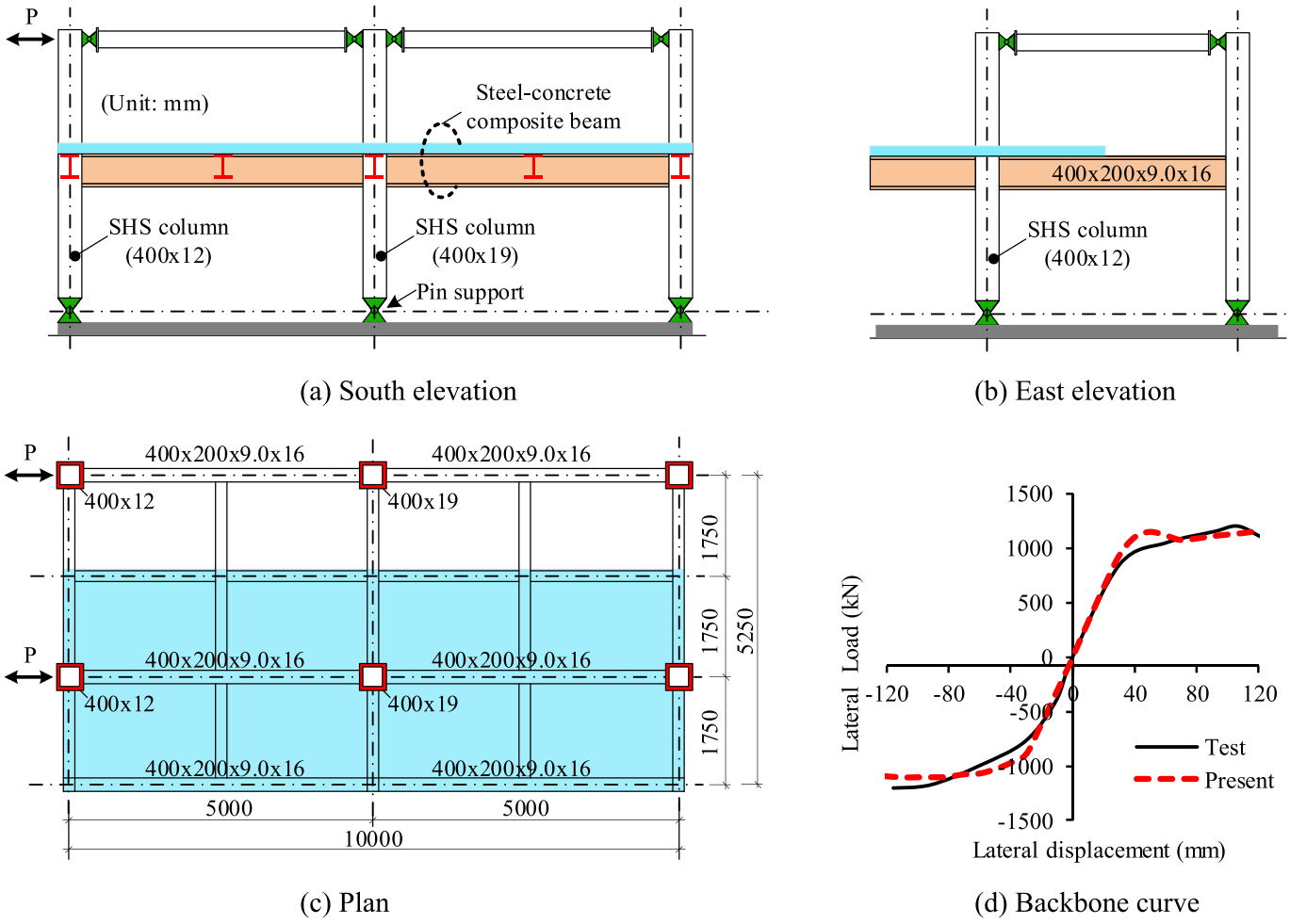


**Fig. 10.** Spatial frame with steel column and steel-concrete composite beams [37].

**Table 3**
Statistical values of variables.

| Properties | Variables | Mean | *CoV* | Distribution | Reference |
|---|---|---|---|---|---|
| Material | Elastic modulus of steel, $E_s$ | 0.993 | 0.034 | Lognormal | [40] |
| | Steel yield strength, $f_y$ | 1.10 | 0.060 | Lognormal | [32,40] |
| | Concrete compressive strength, $f_c$' | 1.08 | 0.150 | Lognormal | [64] |
| Geometry | Diameter of circular steel tube, $D$ | 1.00 | 0.005 | Lognormal | [39] |
| | Width of rectangular steel tube, $B$ | 1.00 | 0.009 | Lognormal | [39] |
| | Height of rectangular steel tube, $H$ | 1.00 | 0.009 | Lognormal | [39] |
| | Thickness of steel tube, $t$ | 0.99 | 0.025 | Lognormal | [39] |
| | Height of steel beam, $h$ | 1.001 | 0.0044 | Normal | [38] |
| | Top flange width of steel beam, $b_{f1}$ | 1.012 | 0.0103 | Normal | [38] |
| | Bottom flange width of steel beam, $b_{f2}$ | 1.015 | 0.0096 | Normal | [38] |
| | Web thickness of steel beam, $t_w$ | 1.055 | 0.0418 | Normal | [38] |
| | Top flange thickness of steel beam, $t_{f1}$ | 0.988 | 0.0436 | Normal | [38] |
| | Bottom flange thickness of steel beam, $t_{f2}$ | 0.998 | 0.0480 | Normal | [38] |
| | Thickness of slab, $t_s$: | | | | |
| | $t_s < 150$ mm | 1.00 | $20/(\sqrt{12}t_s)$ | Normal | [65] |
| | $150 \le t_s \le 400$ mm | 1.00 | $0.04(t_s+350)/(\sqrt{12}t_s)$ | Normal | [65] |
| Load | Dead load, $D_n$ | 1.00 | 0.10 | Normal | [44,45] |
| | Live load, $L_n$ (US code) | 1.00 | 0.25 | Gumbel | [45,46] |
| | $L_n$ (AS code) | 0.60 | 0.35 | Gumbel | [44] |
| | Wind load, $W_{max}/W_{50}$ (US code) | 0.75 | 0.35 | Gumbel | [47] |
| | $W_{max}/W_{50}$ (AS code) | 0.68 | 0.39 | Gumbel | [51,66,67] |

beams by 16-mm-diameter shear studs whose spacing is designed to be small enough to achieve full composite action between the concrete slab and steel beams. The values of concrete compressive strength are 30.7 MPa and 36.6 MPa for slab and columns, respectively. More details can be found in [35]. It can be seen from Figs. 7b and 8b that a good agreement between simulation and experiment has been found.

**Table 4**
Correlations of section dimensions of steel beam [38].

| | $h$ | $b_{f1}$ | $b_{f2}$ | $t_w$ | $t_{f1}$ | $t_{f2}$ |
|---|---|---|---|---|---|---|
| $h$ | 1 | −0.0068 | 0.0534 | 0.0399 | −0.0686 | −0.0989 |
| $b_{f1}$ | −0.0068 | 1 | 0.6227 | −0.2142 | −0.2681 | −0.1456 |
| $b_{f2}$ | 0.0534 | 0.6227 | 1 | −0.2132 | −0.1596 | −0.0423 |
| $t_w$ | 0.0399 | −0.2142 | −0.2132 | 1 | 0.2368 | 0.2451 |
| $t_{f1}$ | 0.0686 | −0.2681 | −0.1596 | 0.2368 | 1 | 0.7634 |
| $t_{f2}$ | −0.0989 | −0.1456 | 0.0423 | 0.2451 | 0.7634 | 1 |

#### 4.1.2. Steel-concrete composite frame with steel columns and composite beams

A planar composite frame, namely F·C, tested by Bursi et al. [36] is taken into consideration. This frame is assembled from a steel column and a composite beam connected to each other by welded connections. The yield strength of steel and the compressive strength of concrete are 300 MPa and 39 MPa, respectively. More details of the geometry and section dimensions are depicted in Fig. 9a. The comparison of the results illustrated in Fig. 9b shows good agreement between simulation and experiment.

#### 4.1.3. Spatial steel-concrete composite frame with steel columns and composite beams

Nakashima et al. [37] tested a full-scale composite frame to investigate the interaction between composite slabs and steel beams subjected to lateral cyclic loads. The thickness of the composite slab is 165 mm, which comprises of 90-mm-thick concrete whose compressive strength is 36 MPa and 75-mm-thick profile steel sheeting. The dimension of the main steel beam is 400 × 200 × 9 × 16 mm with the yield strength of 350 MPa. The geometry of the frame is presented in Fig. 10a. Fig. 10d shows good correlation between simulation and experiment.

### 4.2. Section dimensions and material properties

The uncertainty of the section dimensions of steel beams was evaluated based on the experimental measurements of 371 hot-rolled steel sections conducted by Melcher et al. [38]. The statistical values and the correlation between each parameter of the section are given in Tables 3 and 4, respectively. In the case of CFST columns, the mean and *CoV* of the dimensions of steel tube are taken from [39]. These values will be used in the second generation of Eurocode 3 (EC3). The statistical values of slab thickness are also given in Table 3.

Many studies have been conducted to evaluate the statistical properties of structural steel [40–42]. Galambos and Ravindra [42] found that the distribution of steel yield strength is lognormal with the values of mean and *CoV* around 1.05 and 0.1, respectively, which was evaluated based on the test data and has been utilized in some researches [16,22]. The study conducted by Bartlett et al. [40] in accordance with ASTM A370 [43] found that the mean-to-nominal values of yield strength and elastic modulus are 1.1 and 0.993, respectively, corresponding the values of *CoV* of 0.06 and 0.034. Similar values were also observed from the test data of 4332 specimens based on AS/NZS 3678 [32]. Regarding the uncertainty of concrete properties, only statistical values of concrete compressive strength are considered. More details can be found in Table 3.

### 4.3. Applied loads

The distribution, mean and *CoV* of external loads including dead load

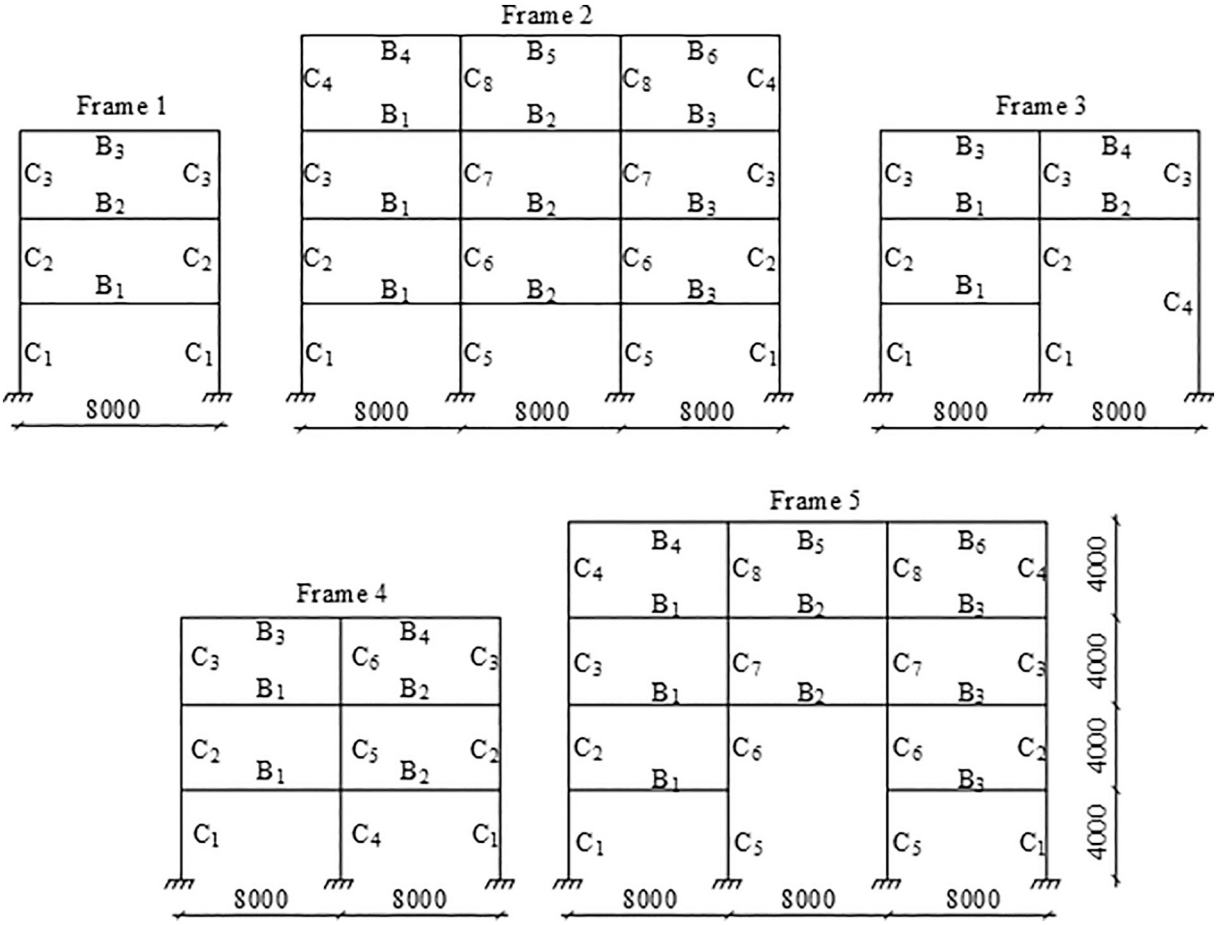


**Fig. 11.** Configurations of investigated steel-concrete composite frames.

**Table 5**
Section dimensions of composite frames under gravity load.

| Specimen | Members | Section dimensions | US code | | | AS code | | |
|---|---|---|---|---|---|---|---|---|
| | | | $\lambda_L$ | $\phi$ | $\beta$ | $\lambda_L$ | $\phi$ | $\beta$ |
| Frame 1 | $C_1$, $C_2$, $C_3$ | 300 × 200 × 4 | 1.711 | 0.584 | 5.01 | 1.760 | 0.568 | 5.93 |
| | $B_1$, $B_2$ | 350 × 150 × 8 × 12 | | | | | | |
| | $B_3$ | 250 × 100 × 8 × 12 | | | | | | |
| Frame 2 | $C_1$, $C_2$, $C_3$, $C_4$ | 350 × 200 × 4 | 1.292 | 0.774 | 3.36 | 1.329 | 0.752 | 4.26 |
| | $C_5$, $C_6$, $C_7$, $C_8$ | 300 × 200 × 3.6 | | | | | | |
| | $B_1$, $B_2$, $B_3$ | 300 × 150 × 8 × 10 | | | | | | |
| | $B_4$, $B_5$, $B_6$ | 220 × 100 × 8 × 10 | | | | | | |
| Frame 3 | $C_1$, $C_2$, $C_3$ | 350 × 200 × 4 | 1.528 | 0.655 | 4.61 | 1.571 | 0.636 | 5.18 |
| | $C_4$ | 350 × 200 × 5 | | | | | | |
| | $B_1$, $B_2$ | 335 × 160 × 8 × 10 | | | | | | |
| | $B_3$, $B_4$ | 265 × 110 × 8 × 10 | | | | | | |
| Frame 4 | $C_1$, $C_2$, $C_3$, $C_4$ | 300 × 200 × 4 | 1.616 | 0.619 | 4.81 | 1.662 | 0.602 | 5.66 |
| | $C_5$, $C_6$ | 200 × 200 × 4 | | | | | | |
| | $B_1$, $B_2$ | 350 × 160 × 8 × 10 | | | | | | |
| | $B_3$, $B_4$ | 250 × 120 × 8 × 10 | | | | | | |
| Frame 5 | $C_1$, $C_2$, $C_3$, $C_4$ | 300 × 200 × 4 | 1.506 | 0.664 | 3.92 | 1.549 | 0.646 | 4.63 |
| | $C_5$, $C_6$ | 350 × 200 × 5 | | | | | | |
| | $C_7$, $C_8$ | 250 × 200 × 4 | | | | | | |
| | $B_1$, $B_2$, $B_3$ | 340 × 150 × 8 × 10 | | | | | | |
| | $B_4$, $B_5$, $B_6$ | 250 × 100 × 8 × 10 | | | | | | |

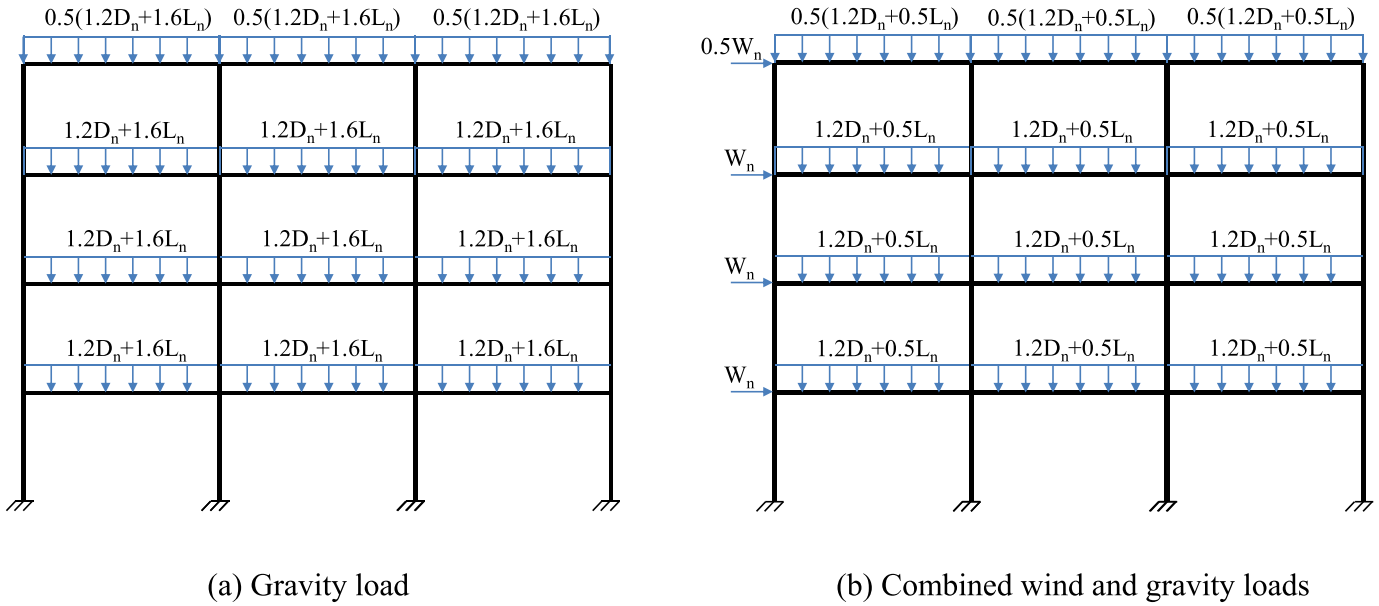


**Fig. 12.** Loading scheme of frame 2 in the case of the US code.

($D_n$), live load ($L_n$) and wind load ($W_n$) are given in Table 3. In the case of $D_n$, similar statistical values have been proposed for both AS and US codes [44,45]. The distribution of $L_n$ is considered as Extreme Type I for the two codes, but the values of mean and *CoV* are different [44–46]. In AS code, the mean of $L_n$ is smaller than that of US code, but its corresponding *CoV* is larger (see Table 3), which is the main factor leading to the difference between the target reliability indices $\beta_T$ in the two codes ($\beta_T = 3.0$ for US code [45,47] and $\beta_T = 3.8$ for AS code [15] based on a 50-year reference period [48]). It should be noted that the statistical values of $L_n$ presented are for the maximum-lifetime live load, and they are also utilized in the case of combined wind and gravity loads.

The characteristics of $W_n$ adopted in the two codes also have some similar features such as the factor of $W_n$ in load combinations, the return period of wind speed and the statistical values of $W_n$. The design wind load in the basic load combinations is taken as $1.0W_n$ for both AS and US codes based on the wind speed with the return period of 500 years ($W_{500}$) [49] and 700 years ($W_{700}$) [50], respectively. The mean-to-nominal value of $W_n$ based on the 50-year return period wind speed ($W_{50}$) is 0.75 for US code (see Table 3), but after converting to the 700-year return period wind speed, this value is 0.47 ($W = 0.75\ W_{50} = 0.75\ W_{700}/1.6 = 0.47\ W_{700}$). The same result was obtained for the case of AS code [51]. Therefore, the mean and *CoV* of $W_n$ are taken as 0.47 and 0.4, respectively, for both two codes.

## 5. Case study of some typical steel-concrete composite frames

In this section, the reliability analysis of some prevalent frames is conducted to determine their system resistance factors when they are subjected to only gravity load and combined wind and gravity loads. The geometry of these frames is depicted in Fig. 11. In each frame, CFST columns are connected to each other by composite beams that comprise of steel beams and 120-mm-thick composite slab. The nominal dead load and live load are 18.51 kN/m, the value of wind load applied to each story is 37.76 kN. The yield strength of steel is 320 MPa, and the

**Table 6**
Section-scale procedure for frame 2 under gravity load.

| Scale factor | Members | Section dimensions | US code | | | AS code | | |
|---|---|---|---|---|---|---|---|---|
| | | | $\lambda_L$ | $\phi$ | $\beta$ | $\lambda_L$ | $\phi$ | $\beta$ |
| 1.0 | $C_1$, $C_2$, $C_3$, $C_4$ | 350 × 200 × 4 | 1.292 | 0.774 | 3.36 | 1.329 | 0.752 | 4.26 |
| | $C_5$, $C_6$, $C_7$, $C_8$ | 300 × 200 × 3.6 | | | | | | |
| | $B_1$, $B_2$, $B_3$ | 300 × 150 × 8 × 10 | | | | | | |
| | $B_4$, $B_5$, $B_6$ | 220 × 100 × 8 × 10 | | | | | | |
| 0.958 | $C_1$, $C_2$, $C_3$, $C_4$ | 335 × 190 × 3.8 | 1.157 | 0.864 | 2.85 | 1.178 | 0.849 | 3.68 |
| | $C_5$, $C_6$, $C_7$, $C_8$ | 290 × 190 × 3.4 | | | | | | |
| | $B_1$, $B_2$, $B_3$ | 290 × 142 × 7.6 × 9.6 | | | | | | |
| | $B_4$, $B_5$, $B_6$ | 210 × 96 × 7.6 × 9.6 | | | | | | |
| 0.933 | $C_1$, $C_2$, $C_3$, $C_4$ | 330 × 180 × 3.6 | 1.058 | 0.945 | 2.48 | 1.088 | 0.919 | 3.35 |
| | $C_5$, $C_6$, $C_7$, $C_8$ | 280 × 180 × 3.2 | | | | | | |
| | $B_1$, $B_2$, $B_3$ | 280 × 140 × 7.2 × 9.2 | | | | | | |
| | $B_4$, $B_5$, $B_6$ | 200 × 95 × 7.2 × 9.2 | | | | | | |

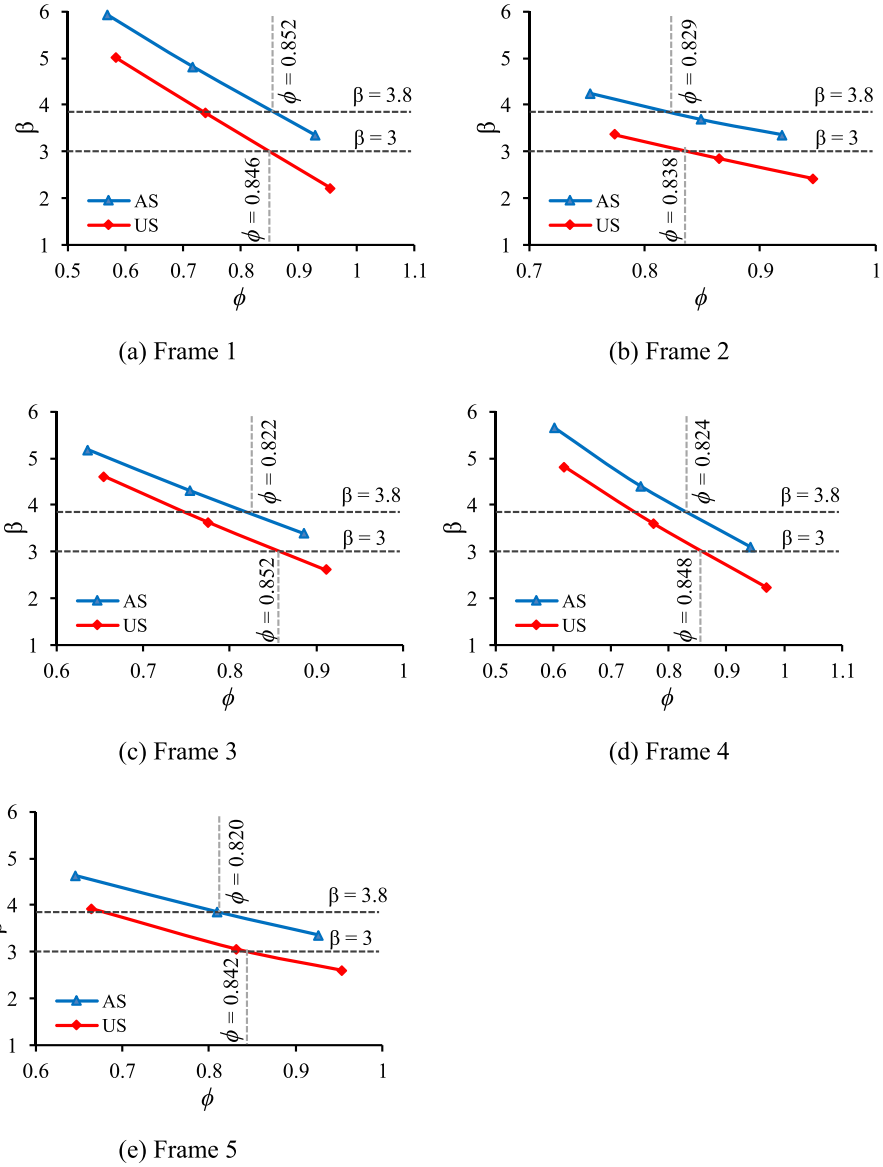


(a) Frame 1 (b) Frame 2

(c) Frame 3 (d) Frame 4

(e) Frame 5

**Fig. 13.** $\beta - \phi$ relationships of investigated frames under gravity load.

**Table 7**
Section dimensions of composite frames under combined wind and gravity loads.

| Specimen | Members | Section dimensions | US code | | | AS code | | |
|---|---|---|---|---|---|---|---|---|
| | | | $\lambda_L$ | $\phi$ | $\beta$ | $\lambda_L$ | $\phi$ | $\beta$ |
| Frame 1 | $C_1$, $C_2$, $C_3$ | 250 × 200 × 4.6 | 1.432 | 0.698 | 4.54 | 1.438 | 0.695 | 4.83 |
| | $B_1$, $B_2$ | 350 × 140 × 8 × 10 | | | | | | |
| | $B_3$ | 280 × 100 × 6 × 8 | | | | | | |
| Frame 2 | $C_1$, $C_2$ | 250 × 200 × 4 | 1.478 | 0.676 | 3.96 | 1.496 | 0.668 | 4.7 |
| | $C_3$, $C_4$, $C_5$, $C_6$, $C_7$, $C_8$ | 200 × 200 × 4 | | | | | | |
| | $B_1$, $B_2$, $B_3$ | 350 × 200 × 8 × 10 | | | | | | |
| | $B_4$, $B_5$, $B_6$ | 250 × 100 × 8 × 10 | | | | | | |
| Frame 3 | $C_1$, $C_2$, $C_3$ | 250 × 200 × 4 | 1.627 | 0.615 | 4.84 | 1.633 | 0.613 | 5.15 |
| | $C_4$ | 300 × 200 × 5 | | | | | | |
| | $B_1$, $B_2$ | 350 × 150 × 8 × 10 | | | | | | |
| | $B_3$, $B_4$ | 250 × 100 × 8 × 10 | | | | | | |
| Frame 4 | $C_1$, $C_2$, $C_3$ | 250 × 200 × 4 | 1.618 | 0.618 | 4.77 | 1.628 | 0.614 | 5.44 |
| | $C_4$, $C_5$, $C_6$ | 200 × 200 × 3.2 | | | | | | |
| | $B_1$, $B_2$ | 350 × 150 × 8 × 10 | | | | | | |
| | $B_3$, $B_4$ | 250 × 100 × 8 × 10 | | | | | | |
| Frame 5 | $C_1$, $C_2$, $C_5$, $C_6$ | 250 × 200 × 4.6 | 1.961 | 0.509 | 4.28 | 1.98 | 0.505 | 5.7 |
| | $C_3$, $C_4$ | 200 × 200 × 4 | | | | | | |
| | $C_7$, $C_8$ | 200 × 200 × 3 | | | | | | |
| | $B_1$, $B_2$, $B_3$ | 350 × 200 × 8 × 10 | | | | | | |
| | $B_4$, $B_5$, $B_6$ | 250 × 100 × 8 × 10 | | | | | | |

**Table 8**
Section-scale procedure for frame 2 under combined wind and gravity loads.

| Scale factor | Members | Section dimensions | US code | | | AS code | | |
|---|---|---|---|---|---|---|---|---|
| | | | $\lambda_L$ | $\phi$ | $\beta$ | $\lambda_L$ | $\phi$ | $\beta$ |
| 1.0 | $C_1$, $C_2$ | 250 × 200 × 4 | 1.478 | 0.676 | 3.96 | 1.496 | 0.668 | 4.71 |
| | $C_3$, $C_4$, $C_5$, $C_6$, $C_7$, $C_8$ | 200 × 200 × 4 | | | | | | |
| | $B_1$, $B_2$, $B_3$ | 350 × 200 × 8 × 10 | | | | | | |
| | $B_4$, $B_5$, $B_6$ | 250 × 100 × 8 × 10 | | | | | | |
| 0.96 | $C_1$, $C_2$ | 240 × 192 × 3.8 | 1.242 | 0.805 | 2.92 | 1.263 | 0.792 | 3.79 |
| | $C_3$, $C_4$, $C_5$, $C_6$, $C_7$, $C_8$ | 192 × 192 × 3.8 | | | | | | |
| | $B_1$, $B_2$, $B_3$ | 335 × 192 × 7.6 × 9.6 | | | | | | |
| | $B_4$, $B_5$, $B_6$ | 240 × 96 × 7.6 × 9.6 | | | | | | |
| 0.92 | $C_1$, $C_2$ | 230 × 184 × 3.6 | 1.015 | 0.986 | 2.22 | 1.042 | 0.959 | 2.94 |
| | $C_3$, $C_4$, $C_5$, $C_6$, $C_7$, $C_8$ | 184 × 184 × 3.6 | | | | | | |
| | $B_1$, $B_2$, $B_3$ | 315 × 184 × 7.4 × 9 | | | | | | |
| | $B_4$, $B_5$, $B_6$ | 230 × 92 × 7.4 × 9 | | | | | | |

**Table 9**
System resistance factors of frames under gravity load.

| Frame | $L_n/D_n$ (US code) | | | | | $L_n/D_n$ (AS code) | | | | |
|---|---|---|---|---|---|---|---|---|---|---|
| | 0.5 | 1.0 | 2.0 | 3.0 | 5.0 | 0.5 | 1.0 | 2.0 | 3.0 | 5.0 |
| Frame 1 | 0.883 | 0.846 | 0.810 | 0.777 | 0.756 | 0.887 | 0.852 | 0.820 | 0.795 | 0.773 |
| Frame 2 | 0.879 | 0.838 | 0.794 | 0.755 | 0.764 | 0.861 | 0.829 | 0.784 | 0.760 | 0.744 |
| Frame 3 | 0.887 | 0.852 | 0.831 | 0.807 | 0.794 | 0.843 | 0.822 | 0.797 | 0.782 | 0.763 |
| Frame 4 | 0.894 | 0.848 | 0.810 | 0.806 | 0.783 | 0.871 | 0.824 | 0.789 | 0.778 | 0.774 |
| Frame 5 | 0.876 | 0.842 | 0.808 | 0.771 | 0.754 | 0.836 | 0.820 | 0.791 | 0.771 | 0.747 |
| Average | 0.884 | 0.845 | 0.811 | 0.783 | 0.770 | 0.860 | 0.829 | 0.796 | 0.777 | 0.760 |

**Table 10**
System resistance factors of frames under combined wind and gravity loads.

| | US code | AS code |
|---|---|---|
| Frame 1 | 0.844 | 0.815 |
| Frame 2 | 0.795 | 0.790 |
| Frame 3 | 0.801 | 0.791 |
| Frame 4 | 0.810 | 0.822 |
| Frame 5 | 0.793 | 0.811 |
| Average | 0.809 | 0.805 |

compressive strength of concrete is 40 MPa.

### 5.1. Steel-concrete composite frames subjected to only gravity load

Firstly, the load factors $\lambda_L$ of composite frames subjected to gravity load are determined using push-down analysis. The total gravity load can be derived from the load combination as $1.2D_n + 1.6L_n$ in US code [50], whilst that of AS code is $1.2D_n + 1.5L_n$ [49]. After that, the reliability analysis is conducted using either MC method or subset simulation. More information about the section dimensions, load factors $\lambda_L$, resistance factors $\phi$ and their corresponding reliability indices are presented in Table 5.

To illustrate the details of the proposed procedure, an example on the reliability analysis of frame 2 subjected to gravity load is presented

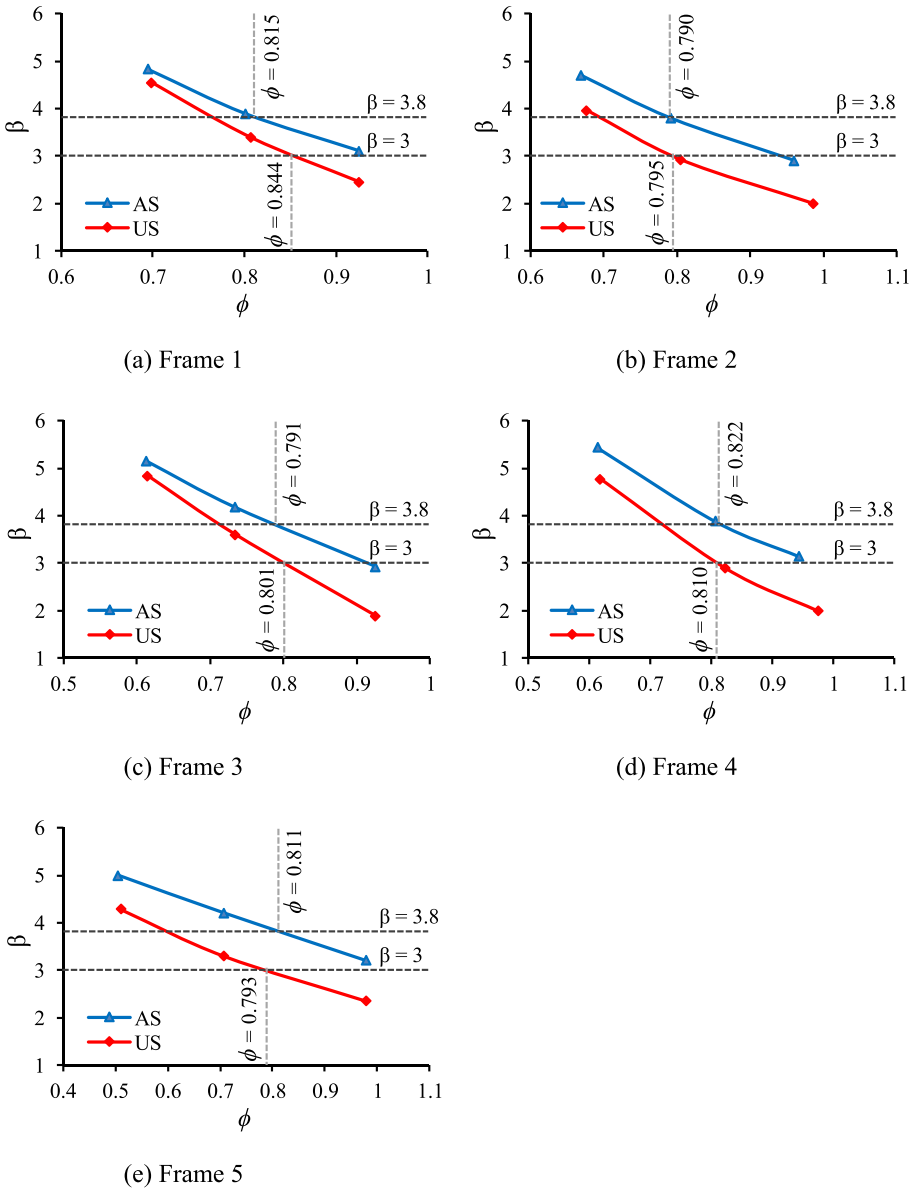


**Fig. 14.** $\beta - \phi$ relationships of investigated frames under combined wind and gravity loads.

herein. The loading scheme and the geometry of this frame are depicted in Fig. 12a. As can be seen in Table 6, the initial section dimensions are scaled down with the ratios from 1.0 to 0.933 that are chosen to achieve the desired load factors $\lambda_L$. The section dimensions of the frame are scaled and adjusted until the corresponding reliability index (which is determined by the reliability analysis), is smaller than the target reliability index taken as $\beta_T = 3$ for US code and $\beta_T = 3.8$ for AS code. The same procedure is applied to other composite frames. The results of frame 2 are depicted in Fig. 13b.

In Fig. 13, the $\beta - \phi$ relationships are presented and the system resistance factors for both US and AS codes are determined. It is obvious that the reliability index decreases when the resistance factor increases. When the resistance factor increases, the cross-section dimensions of the frames are scaled down but the applied loads and all statistical values are remained constant. Hence, the probability of failure is higher, which leads to a smaller reliability index. Fig. 13 also illustrates that the reliability indices obtained from the AS code are always significantly higher than those from the US code. The main reason of this phenomenon is the difference in the mean values of $L_n$. This value is taken as 0.6 in the AS code and is notably smaller than that of the US code. This is also reflected in the choice of the target reliability indices in the two codes.

Based on the target reliability indices of the two codes, the system resistance factors of typical composite frames are determined, these values are in the range from 0.82 to 0.86 in the case frames are subjected to only gravity load (Fig. 13). The most prevalent failure mode in this case is the yielding at the mid-span and the two ends of the composite beams, including the crushing of the concrete slab, since the capacity of CFST columns under gravity loads is prodigiously large. Consequently, the system resistance factors are strongly dependent on the behaviour of the composite beams.

### 5.2. *Composite frames subjected to combined wind and gravity loads*

A similar procedure presented in Section 5.1 is implemented. Firstly, all gravity loads are fully applied, then wind loads are imposed on composite frames to conduct push-over analysis to determine their load factors $\lambda_L$ before running reliability analysis. The results of the analysis, the section dimension and the reliability indices of the investigated

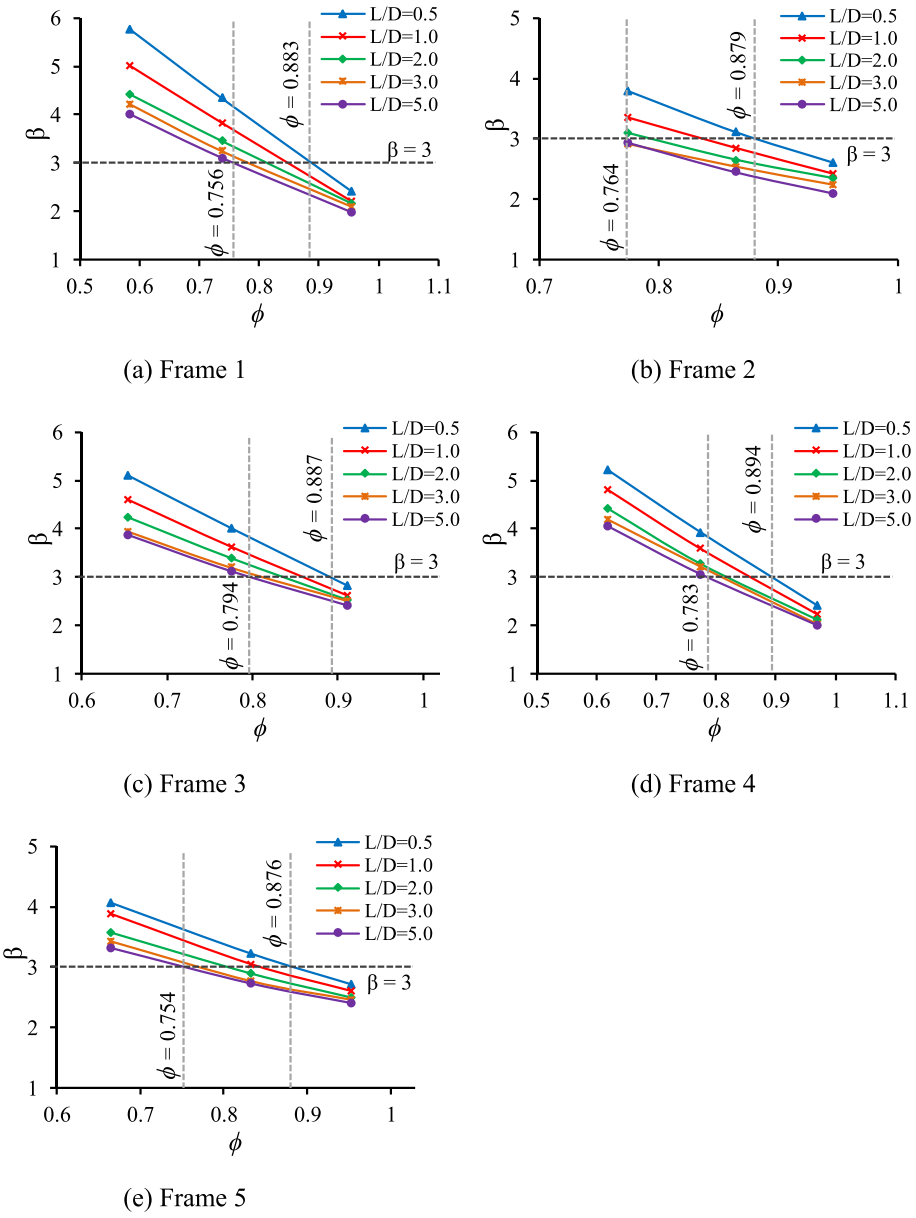


**Fig. 15.** The effect of $L_n/D_n$ on $\beta - \phi$ relationships of frames under gravity load in the case of the US code.

frames are presented in Table 7. In the push-over analysis, the load combinations for the case of combined wind and gravity loads are also considered, which is $1.2D_n + 0.5L_n$ in the US code [50] and $1.2D_n + 0.4L_n$ in the AS code [49]. More details about the loading scheme can be found in Fig. 12b. All frames are designed to fail at the joints where columns are fully yielded, and the beams partially fail.

Fig. 14 illustrates the $\beta - \phi$ curves of composite frames subjected to combined wind and gravity loads. It also shows that the reliability index decreases when the resistance factor increases, which is similar to the case of frames subjected to only gravity load. Also, in Fig. 14, it is obvious that the system resistance factors of all considered frames show less discrepancy. All of them are in the range from 0.79 to 0.84 for both AS and US codes. These values are also in the range given in AS/NZS 2327 [15], which is 0.6 for concrete structures and 0.9 for steel structures. These values are used for LRFD design to account for the variation in strengths due to design assumptions and uncertain variables. When it comes to system design of the steel-concrete composite frames in this study, these uncertainties are explicitly considered and the proposed resistance factors of investigated frames are in the range above, which is obviously reasonable.

## 6. Parametric study

### 6.1. Nominal live load-to-nominal dead load ratio ($L_n/D_n$)

It has been found in some studies that the values of $L_n/D_n$ ratios are in the range from 0.5 to 5 [16,30]. Therefore, many values of $L_n/D_n$ ratios in the range mentioned above including 0.5, 1.0, 2.0, 3.0, 5.0 are considered to investigate their influence on the reliability index and the system resistance factor of frames subjected to only gravity load. The $\beta - \phi$ curves for US and AS codes corresponding to different $L_n/D_n$ ratios are depicted in Figs. 15 and 16, respectively. Fig. 15 shows that when the $L_n/D_n$ ratio increases, the reliability index decreases. This is due to the fact that the *CoV* of live load $L_n$ is much larger than that of dead load $D_n$ (see Table 3). In Fig. 16, the $\beta - \phi$ curves for AS code are illustrated. It is obvious that the same trend with results shown in Fig. 15 for the US code has been observed. However, when the $L_n/D_n$ ratios are adjusted, the fluctuation range of $\beta - \phi$ curves in the case of the AS code is relatively

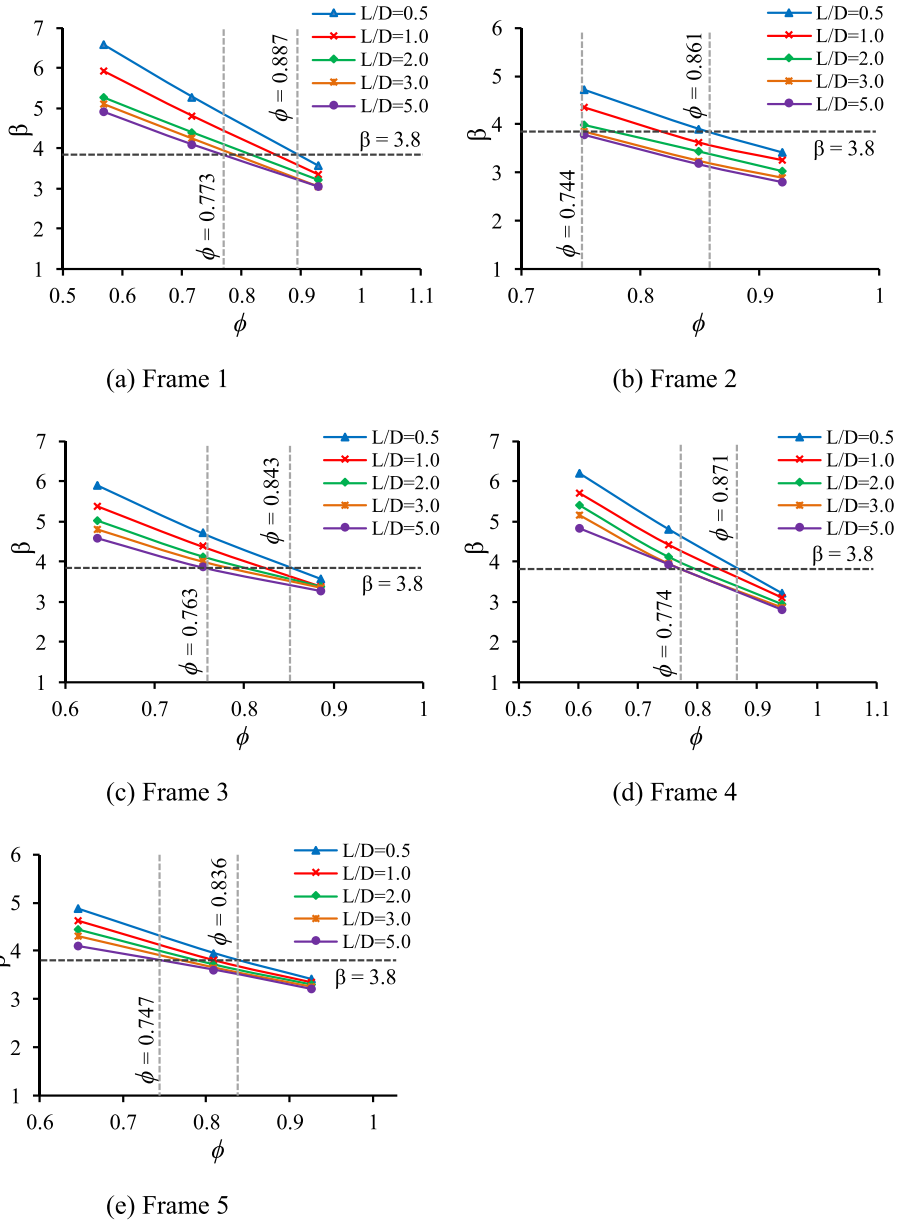


**Fig. 16.** The effect of $L_n/D_n$ on$\beta - \phi$ relationships of frames under gravity load in the case of the AS code.

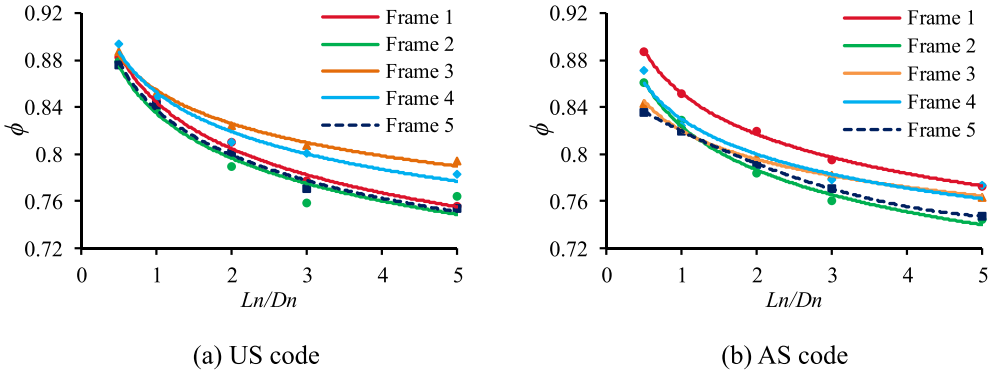


**Fig. 17.** The relationship between $L_n/D_n$ ratios and $\phi$ when frames are under gravity load.

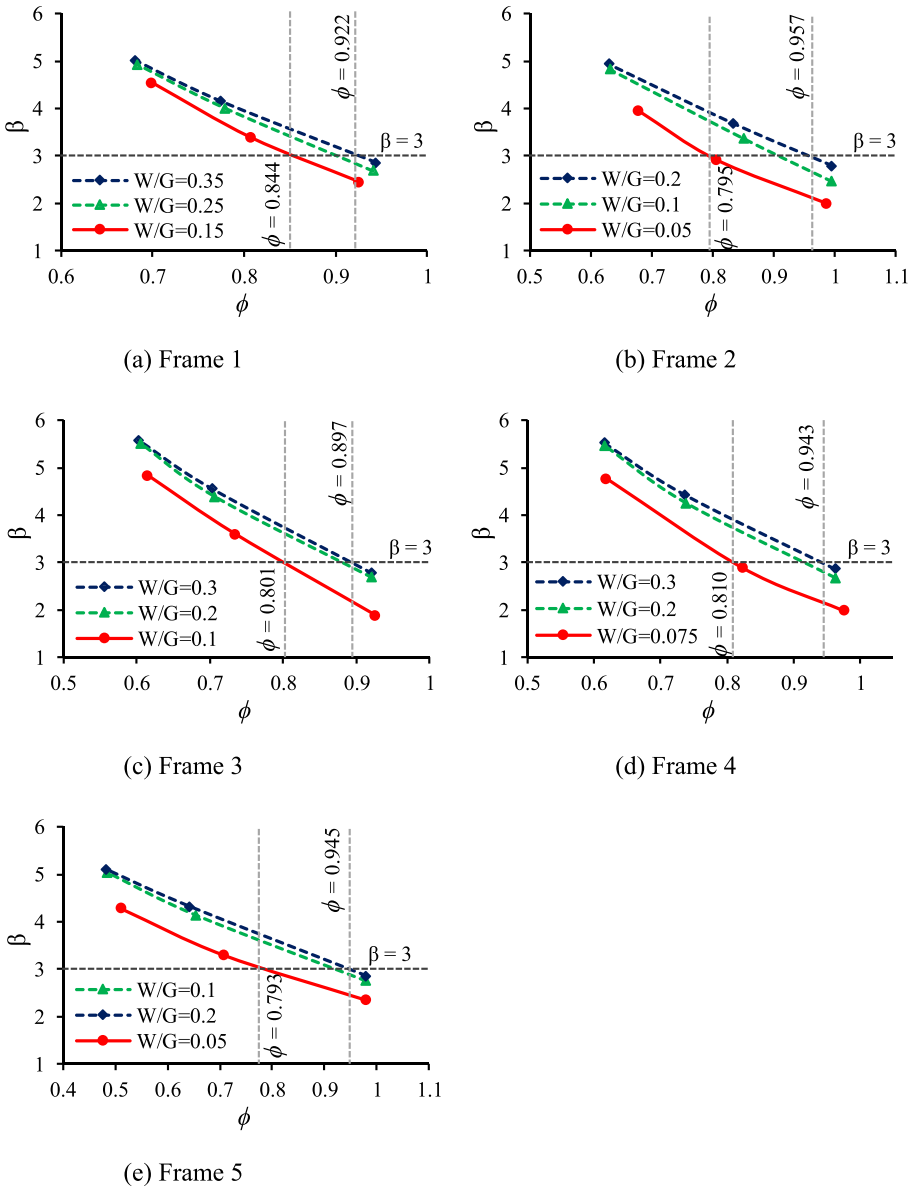


**Fig. 18.** The effect of $W/G$ on$\beta - \phi$ relationships of frames under combined wind and gravity loads in the case of the US code.

smaller than that of the US code, which can be attributed to the smaller mean value of live load $L_n$ in the AS code in comparison to that of the US code. Table 9 and Fig. 17 summarize the system resistance factors for US and AS codes with various values of $L_n/D_n$ ratios. They illustrate that the system resistance factors of frames with different configurations at the same value of $L_n/D_n$ are relatively similar. In addition, these factors decrease significantly from 0.884 to 0.77 in the case of the US code and from 0.86 to 0.76 in the case of the AS code when the $L_n/D_n$ ratio rises from 0.5 to 5.0, which happens due to the reduction of the reliability explained above. Therefore, the value of 0.78, which corresponds to $L_n/D_n = 3.0$, can be taken for the design. However, the designers can refer to Table 9 if needed.

### 6.2. Wind load-to-gravity load ratio (W/G)

In this section, the influence of $W/G$ ratios on the reliability index and the system resistance factor of composite frames is investigated, where $W$ is the total design wind load applied at each story, and $G$ is the total design gravity load. Since the common values of $L_n/D_n$ ratio are less 2.0 [52], the value of 1.0 is chosen for the analysis in this study. Particularly, the values of $D_n$ and $L_n$ are 18.51 kN/m. The nominal wind loads considered in this section are in the range from 37 kN to 80 kN, which corresponds to the popular wind speed from 45 m/s to 66 m/s.

The results of the analysis for US and AS codes are presented in Figs. 18 and 19, respectively. It can be seen from both two figures that the reliability index of investigated frames increases when the $W/G$ ratio rises. This phenomenon occurs because the mean of $W_n$ is substantially smaller than that of $D_n$ and $L_n$, which is 0.47 compared to 1.0 of $D_n$ and $L_n$ (see Section 4.3). Consequently, the influence of gravity loads gradually diminishes when the $W/G$ ratio increases, which leads to a higher reliability index. In Table 10, the values of the system resistance factors of five frames are summarized. Even though the configurations of composite frames are different, the discrepancy in their system resistance factors is negligibly small for both two considered codes, and the value of 0.8 is recommended for the system design of composite frames subjected to combined wind and gravity loads.

### 6.3. Number of stories

In this section, the influence of number of stories is investigated by

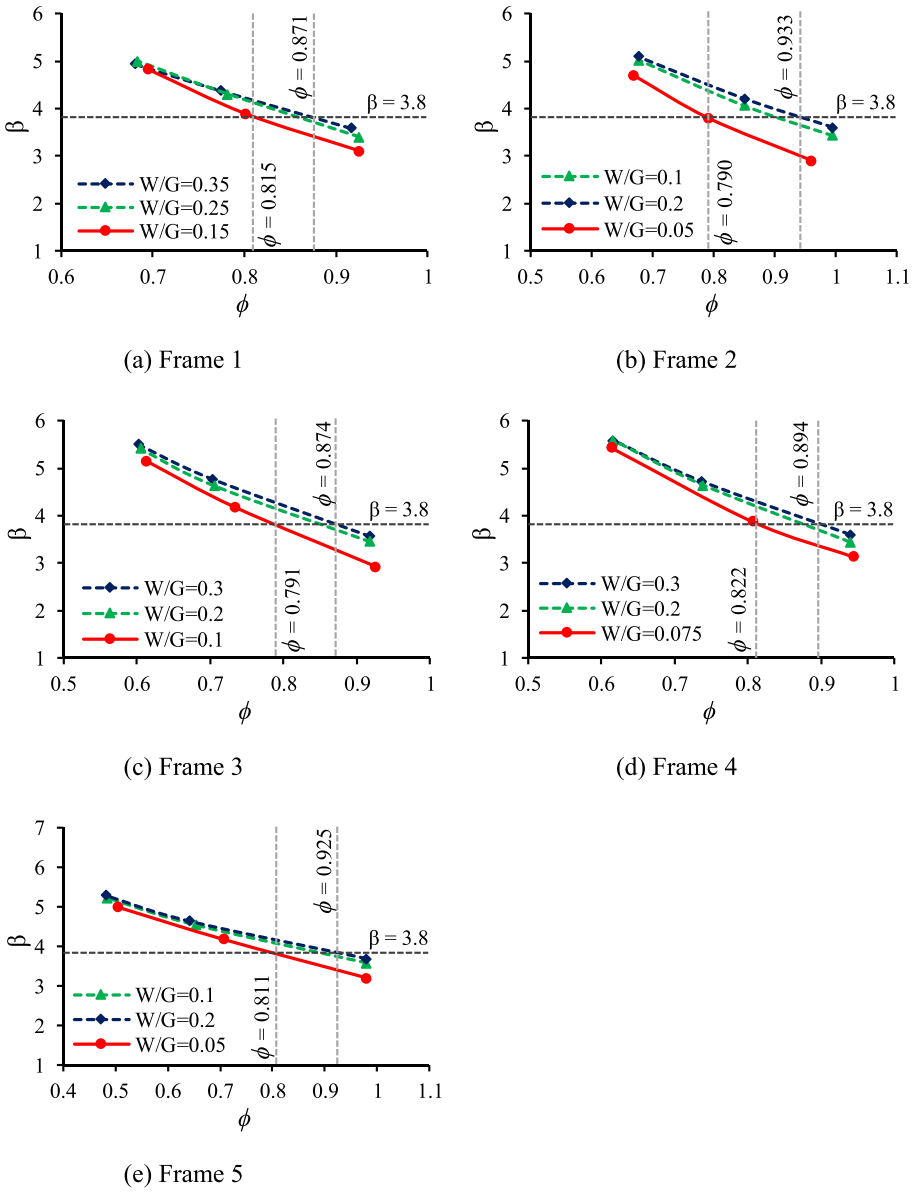


**Fig. 19.** The effect of $W/G$ on$\beta - \phi$ relationships of frames under combined wind and gravity loads in the case of the AS code.

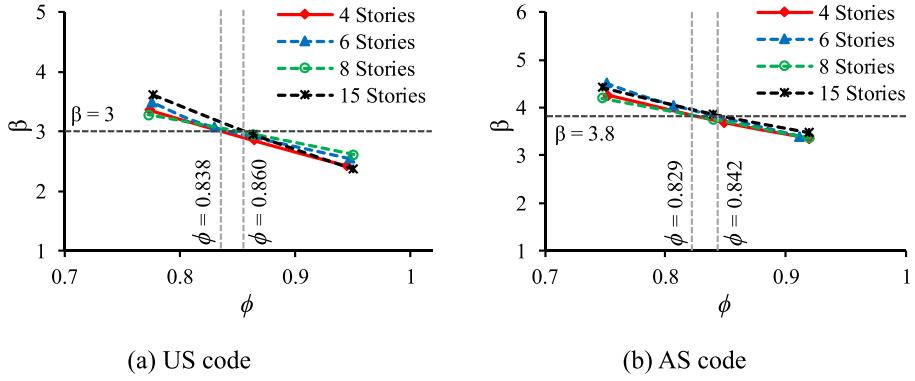


**Fig. 20.** The effect of number of stories on$\beta - \phi$ relationships of frame 2 under gravity load.

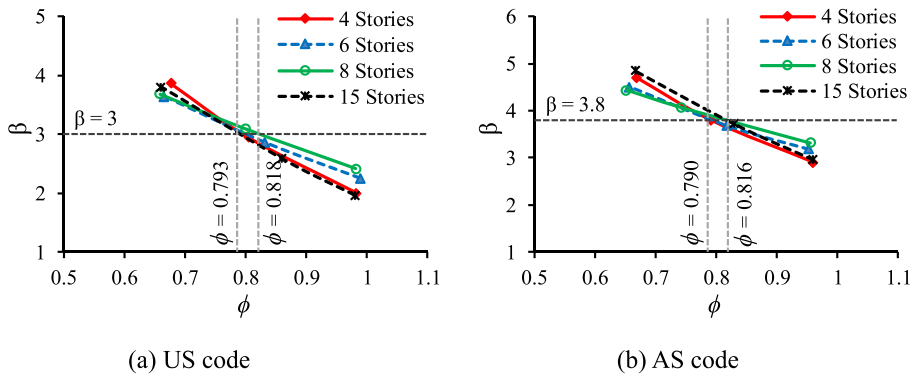


**Fig. 21.** The effect of number of stories on$\beta - \phi$ relationships of frame 2 under combined wind and gravity loads.

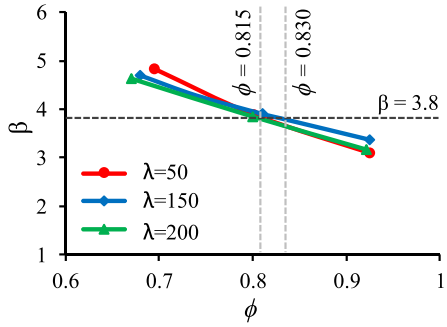


**Fig. 22.** The effect of slenderness ratio on the system resistance factors of frame 1.

considering four scenarios of frame 2 including 4-story frame, 6-story frame, 8-story frame and 15-story frame. To calibrate the reliability and determine the system resistance factors of these frames, the proposed procedure is applied when they are subjected to only gravity load and combined wind and gravity load. The relationships between $\beta$ and $\phi$ for the cases of only gravity load and combined wind and gravity loads are illustrated in Figs. 20 and 21, respectively. As can be seen from these figures, the number of stories has little effect on the system resistance factors of composite frames since these factors show negligible changes when the number of stories is increased. When the frame is subjected to only gravity load, these factors oscillate slightly from 0.838 to 0.860 in the case of the US code and from 0.829 to 0.842 in the case of the AS code, which is under 3%. Similarly, when combined wind and gravity loads are imposed on the investigated frames, the system resistance factors vary in the range from 0.793 to 0.818 for the US code and 0.790 to 0.816 for the AS code, which is around 4%.

### 6.4. *Slenderness ratio*

In traditional LRFD design, the slenderness ratio is considered in the design equations to reflect the geometric nonlinearity and it plays an important role in the calculation of load-carrying capacity of compression members. However, in the system design using nonlinear analysis, the geometric nonlinearity is captured automatically so that less concern about the slenderness ratio is needed. It can be seen in Fig. 22 that the system resistance factors of frame 1 change slightly from 0.815 to 0.830 when the slenderness ratio is increased to 200, which agrees well with what has been explained above.

## 7. Conclusions

This paper proposes an efficient procedure for the reliability analysis of frames with CFST columns and composite beams. In the paper, the MATLAB codes are developed on the basis of subset simulation and MC method. These codes are then integrated with the OpenSees software to evaluate the reliability index of steel-concrete composite frames, and to determine their system resistance factors for both US and AS codes. Many frame configurations under two loading scenarios are investigated. In the case of frames that are subjected to only gravity load, the column strength-to-beam strength ratio is in the range from 0.8 to 1.7 and most columns are stronger than beams to trigger the failure at beams. When frames are subjected to combined wind and gravity loads, this ratio is from 0.5 to 1.2. In this case, the failure mainly occurs at the columns. Although prevalent configurations of composite frames and key parameters are considered, this study only focuses on 2D frames with compact and non-compact sections. In addition, since the frames investigated in this study only have up to three bays and fifteen stories, taller buildings can also be investigated using the proposed procedure. Based on the results of the study, some conclusions can be deduced as following:

(1) The proposed procedure of the reliability analysis is reliable and efficient by using MC method, subset simulation and fibre beam-column elements in OpenSees in predicting the system reliability index of steel-concrete composite frames with CFST columns. The proposed procedure can be applied not only to composite structures in this study but to other kinds of structures as well.
(2) Nonlinear analysis on numerous specimens from experiments has been conducted to determine the statistical values of the model error. From the results of the simulation, it is obvious that the model can capture well the behaviour of steel-concrete composite structures while the mean and *CoV* of the model error are 1.027 and 8.4%, respectively.
(3) The results of the study have demonstrated that the configurations, the slenderness ratio and the number of stories have little influence on the system resistance factors of steel-concrete composite frames with CFST columns. Whilst these parameters are changed, the system resistance factors only fluctuate less than 4%. L/D and W/G ratios show significant effects on the reliability index of a structure. When these parameters are adjusted, the system resistance factors can vary up to 20% in this study.
(4) Through the case study and parametric study, it is recommended that the system resistance factor of investigated steel-concrete composite frames subjected to only gravity load can be taken around 0.78 for both US and AS codes, but a specific value can also be derived from Table 9 if needed. The value of system resistance factor for these frames under combined wind and gravity loads is suggested to be 0.8 for both two codes.

## CRediT authorship contribution statement

**Hau Tran:** Methodology, Validation, Investigation, Visualization, Writing – original draft. **Huu-Tai Thai:** Supervision, Methodology, Conceptualization, Writing – review & editing. **Brian Uy:** Methodology, Conceptualization, Writing – review & editing. **Stephen J. Hicks:** Resources, Writing – review & editing. **Won-Hee Kang:** Resources, Writing – review & editing.

## Declaration of Competing Interest

The authors declare that they have no known competing financial interests or personal relationships that could have appeared to influence the work reported in this paper.

## Acknowledgements

This research was supported by the Australian Research Council (ARC) under its Discovery Scheme (Project No: DP200100112). The financial support is gratefully acknowledged.

## References

[1] L.-H. Han, W. Li, R. Bjorhovde, Developments and advanced applications of concrete-filled steel tubular (CFST) structures: members, J. Constr. Steel Res. 100 (2014) 211–228.
[2] S.J. Hicks, A. Pennington, Partial factors for the design resistance of composite beams in bending, J. Constr. Steel Res. 105 (2015) 74–85.
[3] W.-H. Kang, S.J. Hicks, B. Uy, A. Fussell, Design resistance evaluation for steel and steel-concrete composite members, J. Constr. Steel Res. 147 (2018) 523–548.
[4] J.Y.R. Liew, D.X. Xiong, Ultra-high strength concrete filled composite columns for multi-storey building construction, Adv. Struct. Eng. 15 (2012) 1487–1503.
[5] Z. Tao, U. Katwal, B. Uy, W.-D. Wang, Simplified nonlinear simulation of rectangular concrete-filled steel tubular columns, J. Struct. Eng. 147 (2021) 04021061.
[6] H.-T. Thai, B. Uy, M. Khan, Z. Tao, F. Mashiri, Numerical modelling of concrete-filled steel box columns incorporating high strength materials, J. Constr. Steel Res. 102 (2014) 256–265.
[7] H. Tran, H.-T. Thai, T. Ngo, B. Uy, D. Li, J. Mo, Nonlinear inelastic simulation of high-rise buildings with innovative composite coupling shear walls and CFST columns, Struct. Design Tall Spec. Build. 30 (2021), e1883.
[8] B. Uy, Strength of concrete filled steel box columns incorporating local buckling, J. Struct. Eng. 126 (2000) 341–352.
[9] B. Uy, Strength of short concrete filled high strength steel box columns, J. Constr. Steel Res. 57 (2001) 113–134.
[10] B. Uy, S. Das, Time effects in concrete-filled steel box columns in tall buildings, Struct. Des. Tall Build. 6 (1997) 1–22.
[11] J. Mo, B. Uy, D. Li, H.-T. Thai, H. Tran, A review of the behaviour and design of steel–concrete composite shear walls, Structures 31 (2021) 1230–1253.
[12] H.-T. Thai, T. Ngo, B. Uy, A review on modular construction for high-rise buildings, Structures 28 (2020) 1265–1290.
[13] X. Zhou, J. Liu, Application of steel-tubed concrete structures in high-rise buildings, Int. J. High-Rise Build. 8 (2019) 161–167.
[14] AISC 360-16, Specification for Structural Steel Buildings, 2016.
[15] AS/NZS 2327, Composite Structures—Composite Steel-Concrete Construction in Buildings, 2017.
[16] H. Zhang, S. Shayan, K.J.R. Rasmussen, B.R. Ellingwood, System-based design of planar steel frames, I: Reliability framework, J. Constr. Steel Res. 123 (2016) 135–143.
[17] D. Ziemian Ronald, W. McGuire, Gregory G. Deierlein, Inelastic limit states design. Part I: planar frame studies, J. Struct. Eng. 118 (1992) 2532–2549.
[18] I. Arrayago, K.J.R. Rasmussen, System-based reliability analysis of stainless steel frames under gravity loads, Eng. Struct. 231 (2021), 111775.
[19] C.G. Chiorean, A computer method for nonlinear inelastic analysis of 3D composite steel–concrete frame structures, Eng. Struct. 57 (2013) 125–152.
[20] S.-E. Kim, V.-H. Truong, Reliability evaluation of semirigid steel frames using advanced analysis, J. Struct. Eng. 146 (2020) 04020064.
[21] H.-T. Thai, S.-E. Kim, Nonlinear inelastic analysis of space frames, J. Constr. Steel Res. 67 (2011) 585–592.
[22] H.-T. Thai, B. Uy, W.-H. Kang, S. Hicks, System reliability evaluation of steel frames with semi-rigid connections, J. Constr. Steel Res. 121 (2016) 29–39.
[23] S.G. Buonopane, B.W. Schafer, Reliability of steel frames designed with advanced analysis, J. Struct. Eng. 132 (2006) 267–276.
[24] J.B. Cardoso, J.R. de Almeida, J.M. Dias, P.G. Coelho, Structural reliability analysis using Monte Carlo simulation and neural networks, Adv. Eng. Softw. 39 (2008) 505–513.
[25] I. Papaioannou, W. Betz, K. Zwirglmaier, D. Straub, MCMC algorithms for subset simulation, Probabilistic Eng. Mech. 41 (2015) 89–103.
[26] H.-T. Thai, S. Thai, T. Ngo, B. Uy, W.-H. Kang, S.J. Hicks, Reliability considerations of modern design codes for CFST columns, J. Constr. Steel Res. 177 (2021), 106482.
[27] J. Jafari-Asl, S. Ohadi, M.E.A.B. Seghier, N.-T. Trung, Accurate structural reliability analysis using an improved line-sampling-method-based slime mold algorithm, ASCE-ASME J. Risk Uncertain. Eng. Syst. Part A 7 (2021) 04021015.
[28] B. Keshtegar, M.E.A.B. Seghier, E. Zio, J.A.F.O. Correia, S.-P. Zhu, N.-T. Trung, Novel efficient method for structural reliability analysis using hybrid nonlinear conjugate map-based support vector regression, Comput. Methods Appl. Mech. Eng. 381 (2021), 113818.
[29] A.T. Beck, W.L.A. de Oliveira, S. De Nardim, A.L.H.C. ElDebs, Reliability-based evaluation of design code provisions for circular concrete-filled steel columns, Eng. Struct. 31 (2009) 2299–2308.
[30] S. Chen, H. Zhang, C. Hou, L.-H. Han, T.-M. Mu, Reliability calibration for the design of multiple-chord CFST trusses by advanced analysis, Struct. Saf. 89 (2021), 102051.
[31] W.H. Kang, B. Uy, Z. Tao, S. Hicks, Design strength of concrete-filled steel columns, Adv. Steel Constr. 11 (2014) 20.
[32] H. Liu, System Reliability Calibrations for the Direct Design Method of Planar Steel Frames with Partially Restrained Connections [PhD thesis], Faculty of Engineering and IT: University of Sydney, 2019.
[33] A.S. Nowak, K.R. Collins, Reliability of Structures, CRC press, 2012.
[34] S.-K. Au, J.L. Beck, Estimation of small failure probabilities in high dimensions by subset simulation, Probabilistic Eng. Mech. 16 (2001) 263–277.
[35] N. Jianguo, H. Yuan, Y. Weijian, F. Jiansheng, Seismic behavior of CFRSTC composite frames considering slab effects, J. Constr. Steel Res. 68 (2012) 165–175.
[36] O.S. Bursi, G. Gramola, Behaviour of composite substructures with full and partial shear connection under quasi-static cyclic and pseudo-dynamic displacements, Mater. Struct. 33 (2000) 154–163.
[37] M. Nakashima, T. Matsumiya, K. Suita, F. Zhou, Full-scale test of composite frame under large cyclic loading, J. Struct. Eng. 133 (2007) 297–304.
[38] J. Melcher, Z. Kala, M. Holický, M. Fajkus, L. Rozlívka, Design characteristics of structural steels based on statistical analysis of metallurgical products, J. Constr. Steel Res. 60 (2004) 795–808.
[39] M. Knobloch, A. Bureau, U. Kuhlmann, L.S. da Silva, H.H. Snijder, A. Taras, et al., Structural member stability verification in the new part 1-1 of the second generation of Eurocode 3, Steel Constr. 13 (2020) 98–113.
[40] F.M. Bartlett, R.J. Dexter, M.D. Graeser, J.J. Jelinek, B.J. Schmidt, T.V. Galambos, Updating standard shape material properties database for design and reliability, Eng. J. 40 (2003) 2–14.
[41] R.J. Dexter, M.D. Graeser, M.K. Saari, C. Pascoe, C.A. Gardner, T.V. Galambos, Structural Shape Material Property Survey, University of Minnesota, Minneapolis, MN, 2000.
[42] V. Galambos Theodore, Mayasandra K. Ravindra, Properties of steel for use in LRFD, J. Struct. Div. 104 (1978) 1459–1468.
[43] ASTM A370 - 97a, Standard Test Methods and Definitions for Mechanical Testing of Steel Products, 1997.
[44] European Commission, Development of Skills Facilitating Implementation of Eurocodes, Handbook 2 - Reliability Background: The Leonardo da Vinci Pilot Project CZ/02/B/F/PP-134007, 2005.
[45] T.V. Galambos, Load and resistance factor design, Eng. J. 18 (1981) 74–82.
[46] B. Ellingwood, G. MacGregor James, V. Galambos Theodore, C.A. Cornell, Probability based load criteria: load factors and load combinations, J. Struct. Div. 108 (1982) 978–997.
[47] P. McAllister Therese, N. Wang, Bruce R. Ellingwood, Risk-informed mean recurrence intervals for updated wind maps in ASCE 7-16, J. Struct. Eng. 144 (2018) 06018001.
[48] ISO 2394, General Principles on Reliability for Structures, 1998.
[49] AS/NZS 1170.0:2002, Structural design actions and general principles, Australian Standard (2002).
[50] ASCE/SEI 7-16, Minimum design loads and associated criteria for buildings and other structures, American Standard (2016).
[51] F. Sena Cardoso, H. Zhang, K.J.R. Rasmussen, S. Yan, Reliability calibrations for the design of cold-formed steel portal frames by advanced analysis, Eng. Struct. 182 (2019) 164–171.
[52] B. Ellingwood, G. MacGregor James, V. Galambos Theodore, C.A. Cornell, Development of a Probability Based Load Criterion for American National Standard A58: Building Code Requirements for Minimum Design Loads in Buildings and Other Structures, National Bureau of Standards, Washington DC, 1980.
[53] K. Udagawa, H. Mimura, Behavior of composite beam frame by pseudodynamic testing, J. Struct. Eng. 117 (1991) 1317–1334.
[54] S.R.S. Kumar, M.S. Smitha, Steel–concrete composite flange plate connections: cyclic performance and tests, J. Constr. Steel Res. 82 (2013) 216–222.
[55] European Commission, Applicability of Composite Structures to Sway Frames, 2003.
[56] F. Benussi, C. Bernuzzi, S. Noè, Experimental Analysis of Semi-Rigid Composite Frames, 1996.
[57] T.-S. Eom, H.-G. Park, C.-H. Lee, J.-H. Kim, I.-H. Chang, Behavior of double skin composite wall subjected to in-plane cyclic loading, J. Struct. Eng. 135 (2009) 1239–1249.
[58] J.-F. Wang, G.-Q. Li, Testing of semi-rigid steel–concrete composite frames subjected to vertical loads, Eng. Struct. 29 (2007) 1903–1916.
[59] J. Wang, J. Wang, H. Wang, Seismic behavior of blind bolted CFST frames with semi-rigid connections, Structures 9 (2017) 91–104.
[60] Y. Tagawa, B. Kato, H. Aoki, Behavior of composite beams in steel frame under hysteretic loading, J. Struct. Eng. 115 (1989) 2029–2045.

[61] U.I. Dissanayake, I.W. Burgess, J.B. Davison, Modelling of plane composite frames in unpropped construction, Eng. Struct. 22 (2000) 287–303.
[62] L.-H. Han, W.-D. Wang, X.-L. Zhao, Behaviour of steel beam to concrete-filled SHS column frames: finite element model and verifications, Eng. Struct. 30 (2008) 1647–1658.
[63] A. Plumier, J.B. Schleich, Seismic resistance of steel and composite frame structures, J. Constr. Steel Res. 27 (1993) 159–176.
[64] F.M. Bartlett, G.M. James, Statistical analysis of the compressive strength of concrete in structures, ACI Mater. J. 93 (1996).
[65] EN 13670, Execution of Concrete Structures, 2009.
[66] J.D. Holmes, Wind loads and limit states design, Inst. Eng. (Australia) Civ. Eng. Trans. CE2 (1985) 21–26.
[67] L. Pham, J.D. Holmes, R.H. Leicester, Safety indices for wind loading in Australia, J. Wind Eng. Ind. Aerodyn. 14 (1983) 3–14.